Summer 2018

Effects of Automated Fiber Placement on High Strain Rate Compressive Response of Advanced Composites

Alexander Trochez
Old Dominion University

EFFECTS OF AUTOMATED FIBER PLACEMENT DEFECTS ON HIGH STRAIN RATE COMPRESSIVE RESPONSE OF ADVANCED COMPOSITES

by

Alexander Trochez
B.S May 2013, Grambling State University

A Thesis Submitted to the Faculty of
Old Dominion University in Partial Fulfillment of the
Requirements for the Degree of

MASTER OF SCIENCE

MECHANICAL AND AEROSPACE ENGINEERING

OLD DOMINION UNIVERSITY
August 2018

Approved by:

Dipankar Ghosh (Director)

Oleksandr Kravchenko (Member)

Chauncey Wu (Member)

ABSTRACT

EFFECTS OF AUTOMATED FIBER PLACEMENT DEFECTS ON HIGH STRAIN RATE COMPRESSIVE RESPONSE OF ADVANCED COMPOSITES

Alexander Trochez
Old Dominion University, 2018
Director: Dr. Dipankar Ghosh

Automated Fiber Placement (AFP) technology shows great promise in manufacturing carbon fiber composite structures. However, intermittent defects occur in the process that can affect the overall mechanical performance of the structure. The aim of this work is to investigate the effects of deliberately placed principal defects (Gap, Overlap, and Fold) on the compressive response under quasistatic (strain rate ~10^{-3} s^{-1}) and dynamic (strain rate ~10^{3} s^{-1}) loading conditions. The controlled defects were placed at the laminate level in different orientations and depths. High strain rate compression experiments were conducted using a split Hopkinson pressure bar (SHPB) set up, whereas an electrohydraulic testing machine was employed to perform quasistatic compression tests. Three 24 ply carbon fiber panel structures (quasi-isotropic, unidirectional, and quasi-isotropic with deliberately placed defects) were manufactured using AFP with IM7-8552 material, for testing and developing comparative baseline measurements. Results show that there is a significant effect of deliberately placed defects on the compressive strength of composites. Aside from the thickness orientation, the laminate directions along the side of the defect demonstrated a higher peak strength than in the traverse direction. The experimental results revealed a decrease in compressive strength; however, the defects along the fiber direction disturbed the laminate matrix, causing the cured resin in the fiber matrix to slightly strengthen the samples.

ACKNOWLEDGMENTS

There are many people who have contributed to the successful completion of this thesis. I extend many, many thanks to my committee members and colleagues for their patience and hours of guidance on my research and editing of this manuscript. The untiring efforts of my major advisors deserve special recognition.

TABLE OF CONTENTS

Page

LIST OF FIGURES

Figure Page

CHAPTER 1

INTRODUCTION

Advanced composite materials and structures are widely recognized throughout multiple industries such as, but not limited to, transportation, military, construction, and medical. Advanced composites are materials that contain carbon fibers embedded in a resin matrix. The widespread use of composites contributes to reduced weight, maintenance requirements, and also increase in strength performance and reliability of different systems. Today's automated manufacturing technologies have satisfied the needs in fabricating composite components for current industry requirements. However, there is a higher demand in weight and performance requirements for future models, which will require further advancements, including development of more advanced materials and structures and more efficient and affordable manufacturing technologies and fabrication processes. A major advancement in computer-numerical-control machine tools has allowed scientists and engineers to adopt this technology in composites, by creating tow placement or Automated Fiber Placement (AFP) technology. AFP technology minimizes human error, by creating precise repeatable, tension independent processes, enabling carbon fiber placement at any angle. This allows high pattern complex structures to be developed, while improving the composite structure quality, providing excellent mechanical properties.

1.1 Problem

In order to manufacture complex shapes or parts, misalignments are induced on the band edges, which introduce defects. In addition, the material and machine tolerances induce defects that cannot be removed, because they are a part of the processing. Furthermore, missing, twisted, or spliced tows are sometimes laid down during manufacturing; they create uncertainties and

must be repaired during the process. These defects can alter the performance of these advanced composite structures by a reduction in strength. Another idea that was developed in this study will investigate a correlation between the placement of these defects in the ply thickness, and any reduction in strength.

The overall aim of this thesis is to study the roles of controlled defects at different through-thickness locations using quasi-static and high-strain rate response testing of advanced composites. With this aim, the hypothesis for this study based on different journal articles, is that the defects will reduce the strength of the panels. The goal is to find out how much reduction will occur with the embedded defects and whether the different through thickness locations play a significant role in further reducing the strength.

1.2 Purpose

The purpose of this research is to use Automated Fiber Placement technology to investigate defects in its manufacturing process. Recent technological developments have increased both the affordability and utility of Automated Fiber Placement.

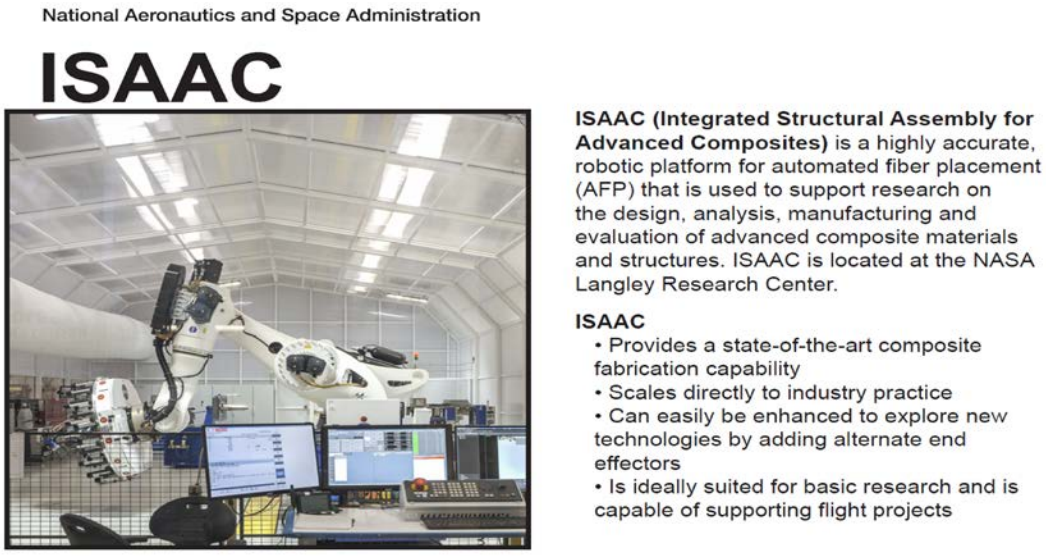

Figure 1: ISAAC Overview [1]

This capability being acquired by NASA Langley Research Center is named ISAAC, or Integrated Structural Assembly of Advanced Composites. The AFP end effector provides a highly mature, state-of-the-art, initial operating capability for ISAAC that is fully compatible with the composites manufacturing processes used throughout the aerospace industry. In fact, the same type of AFP end effector is also used on other mobility platforms to manufacture large composite primary structures. [1]. With this recently acquired technology, NASA scientists, engineers and technicians have been using ISAAC to fabricate flat panels for different projects on center. While using extra materials for verification and validation of these flat panels using the AFP end effector, an interesting subject matter began to culminate to determine the strength of these panels, by testing and characterization using experimental instruments at Old Dominion University. With the lack of literature in this field, the motivation was to understand the intricacies in the manufacturing process of AFP, and use this technology to investigate the strength of carbon fiber panels manufactured in different ways with different defects.

Literature Review

2.1 Mechanical Responses of advanced composites under high strain rates

In this work, Körber presents an investigation of strain rate effects on the elastic, plastic and strength properties of unidirectional carbon-epoxy composites. He uses the carbon-epoxy material system IM7-8552 to develop a 12 ply unidirectional panel and cuts it into 23x7x1.5 mm samples for quasi-static and high strain rate experiments. These tests were performed in the longitudinal and transverse compressive direction.

Test	Strain Rate $\dot{\varepsilon}$ [s^{-1}]	Modulus E_{1C}^{dyn} [MPa]	Strength X_C^{dyn} [MPa]
DYN-1	118	138350	1365
DYN-2	63	168590	1409
DYN-3	77	160250	1432
DYN-4	97	155320	1427
DYN-5	110	137550	1453
Mean	93	152012	1417
STDV	23	13688	33
CV (%)	25.0	9.0	2.3

Figure 2: Dynamic experimental results [2]

The high strain rate testing was conducted by using a split-Hopkinson pressure bar. His work also includes optimizing this testing instrument by means of systematic pulse shaping and direct strain measurements on the specimen, using strain gauges. All of his high strain rate tests were performed under dynamic stress equilibrium and at near constant strain rates. As a result itwas possible to obtain both reliable elastic and strength properties from the measured dynamic stress-strain response. From the latter tests, the quasi-static and dynamic in-plane shear response was determined and the yield strength and failure envelopes for combined transverse compression and in-plane shear loading were established and compared with a state-of-the-art failure criterion.

Test	Strain Rate $\dot{\varepsilon}$ [s^{-1}]	Modulus E_{1C}^{qs} [MPa]	Strength X_C^{qs} [MPa]
QS-1	7.2×10^{-5}	160992	1018
QS-2	3.6×10^{-4}	152485	1002
QS-3	3.6×10^{-4}	148167	946
QS-4	3.6×10^{-4}	-	1023
QS-5	3.6×10^{-4}	156301	1093
Mean	-	154486	1017
STDV	-	5464	53
CV (%)	-	3.5	5.2

Figure 3: Quasi-static experimental results [2]

At the strain rates studied in this work, no strain rate effect was observed for the longitudinal compressive modulus, whereas a moderate and consistent increase, with increasing loading rate, was found for the transverse compressive, in-plane shear and off-axis compressive moduli. More significant and again consistent strain rate effects were observed for the longitudinal compressive strength, and for the transverse compressive, in-plane shear and off-axis compressive yield and failure strengths. As for the compression tests, the experimental failure envelope was compared with advanced failure criteria. [2]

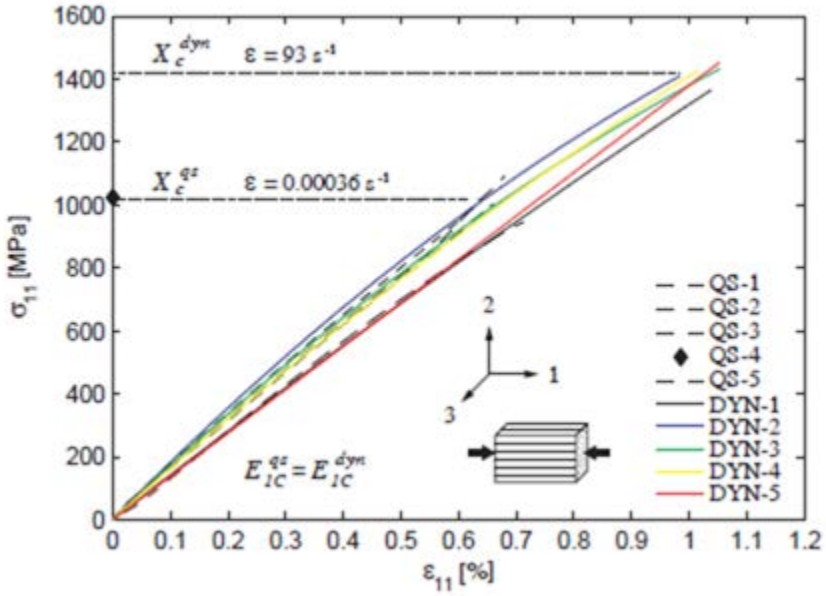

Figure 4: Comparison of quasi-static and dynamic longitudinal compressive stress strain response [2]

Figure 4 provides the overall comparison data for this study for the stress conditions.

2.2 Effect of strain rate on the mechanical properties of carbon/epoxy composites under quasi-static and dynamic loadings

With this journal article, Li conducts investigations on warp-knitted and plain weave carbon fabric composites made under quasi-static and dynamic strain rates, mainly focusing on the effect of strain rate on the tensile and compressive strength of the composite. The researcher does this by testing (6 x 6 x 6) mm samples for the quasi-static portion and (6 x 8 x 6) mm samples for the dynamic testing using a [_45_/0_/45_/90_] 6s stacking sequence.

Item	Warp-knitted fabric		Plain weave fabric	
	Compressive strength/MPa	Fracture strain/%	Compressive strength/MPa	Fracture strain/%
Specimen 1#	282	1.34	235	1.65
Specimen 2#	292	1.59	256	1.58
Specimen 3#	256	1.18	246	1.37
Specimen 4#	337	1.46	260	1.62
Specimen 5#	286	1.52	214	1.53
Specimen 6#	259	1.38	209	1.48
Specimen 7#	296	1.44	253	1.56
Average	287	1.42	239	1.54
Dispersion/%	8.71	8.68	7.91	5.66

Figure 5: Quasi-static compressive results [3]

The strain rate was 0.5 s-1for quasi-static tests performed on a universal testing machine as shown in figure 5, whereas it ranged from approximately 200 s-1to 2300 s-1 for the dynamic testing as shown in figure 6.

Item	Warp-knitted fabric		Plain weave fabric	
	Compressive strength/MPa	Strain Rate/s^{-1}	Compressive strength/MPa	Strain Rate/s^{-1}
Specimen 1#	222	221	237	260
Specimen 2#	231	320	327	416
Specimen 3#	252	353	314	597
Specimen 4#	246	427	310	624
Specimen 5#	228	641	315	649
Specimen 6#	209	864	278	788
Specimen 7#	208	969	261	901
Specimen 8#	253	1332	384	1337

Figure 6: Dynamic compressive results [3]

The test results show that the tensile strength increased with increasing strain rate for both types of fabrics, whereas the effect of strain rate was negligible for the compressive strength.

2.3 Influence of embedded gap and overlap fiber placement defects on the microstructure and shear and compression properties of carbon–epoxy laminates

This paper presents results from an experimental study of the influence of embedded defects created during automated fiber tape placement, on the mechanical properties of carbon/epoxy composites. Two stacking sequences have been examined, [(-45°/+45°)3/-45°] and [90°_4/0°_3/90°_4], in which gaps and overlaps have been introduced during fiber placement. These materials have been cured in an autoclave either with or without a caul plate, then analyzed by ultrasonic C-scan. The microstructures were characterized by scanning electron microscopy. In-plane shear tests were performed on the ±45° laminates and showed that the use of a caul plate does not affect mechanical behavior of plies in the embedded defect region. Compression tests were performed on 0°/90° laminates and in this case the presence of a caul plate is critical during polymerization as it prevents thickness variations and allows defects to heal.

	Shear		Compression	
	Modulus (GPa)	Strength (MPa)	Modulus (GPa)	Strength (MPa)
Manual layup – without embedded defect – with caul plate	5.19 ± 0.08	68.2 ± 1.0	40.01 ± 4.18	375.2 ± 32.2
AFP layup – gap 0.5 mm – with caul plate	4.77 ± 0.12	64.1 ± 1.7	39.25 ± 4.31	420.8 ± 24.9
AFP layup – gap 3.175 mm – with caul plate	4.59 ± 0.07	59.3 ± 4.0	39.51 ± 7.63	368.8 ± 16.9
AFP layup – overlap 3.175 mm – with caul plate	4.88 ± 0.15	67.0 ± 2.2	62.85 ± 11.23	376.4 ± 26.3
AFP layup – gap 0.5 mm – without caul plate	4.92 ± 0.10	63.8 ± 1.3	35.64 ± 4.24	392.0 ± 17.0
AFP layup – gap 3.175 mm – without caul plate	4.45 ± 0.11	54.6 ± 2.1	38.14 ± 5.60	310.0 ± 31.2
AFP layup – overlap 3.175 mm – without caul plate	4.95 ± 0.13	63.3 ± 1.3	10.55 ± 0.72	179.6 ± 9.0

Figure 7: Embedded defect results

From this paper, the 3.175mm gap produced a 12% drop in strength using a caul plate during the autoclave processing phase and a 20% reduction in strength without a plate.

The Overlap shows similar results as the gap using a caul plate but the strength has experienced a significant 55% reduction in strength without a plate.

2.4 Composites for Exploration Upper stage

In this study, solid laminate panels were fabricated from IM7/8552-1 and tested for equivalence to data reported within the NCAMP database. Panels were made by hand lay-up at NASA Glenn and by automated fiber placement at NASA Langley and NASA Marshall. The panel dimensions were determined by the dimensions and quantity of coupons required for mechanical tests. A total of 16 panels were made to meet the coupon requirements. The key difference between these three sets of panels was the use of 1/4-inch-wide slit tape at NASA Langley, 1/2-inch-wide slit tape for fiber placement at NASA Marshall, and 12-inch-wide unidirectional prepreg for hand layup at NASA Glenn.

Unnotched Compression Strength						
Panel	CTD		RTD		ETW	
	ksi	CV	ksi	CV	ksi	CV
NCAMP Database	n/a	n/a	87	9.3	57.7	11
HXL-H12-**GRC**-A-UNC1-B	112.8	4.50	95.1	4.3	59.6	12.6
HXL-H12-**GRC**-A-M-OHC1-LV	117.5	3.3	96.2	5.6	59.9	10.4
HXL-H12-**GRC**-A-M-OHC1-SR	118.9	2.9	100.3	2.7	61.1	5.1
HXL-H12-**LaRC**-A-M-OHC1	119.8	3.7	94.1	2.2	57.9	7.5
HXL-H12-**MSFC**-A-M-OHC1	114.3	5.3	97.7	3.3	62.1	2.7

Figure 8: Unnotched Compression Strength CEUS results

After fabricating the 16 ply panels, multiple tests were conducted. This review will focus on the unnotched compression test conducted, using the ASTM D6641 standard. The compression test results are shown in figure 8.

METHODOLOGY

The ISAAC system at the NASA Langley Research Center was used to fabricate three panels from 1/4-inch-wide IM7/8552-1 graphite/epoxy prepreg slit tape. The panels included a pristine quasi-isotropic 24-ply panel (12 x 12inches) using a [45/0/-45/90]3s stacking sequence, unidirectional [0] 24-ply panel (12 x 12 inches), and a defect quasi-isotropic 24-ply panel (12 x 24 inches) using the same stacking sequence as the pristine panels for a baseline.

3.1 Materials

Hexcel's IM7/8552-1 prepreg tape was selected as the structural test article (STA) face-sheet material based on its amenability to fiber placement. Hexcel's 8552-1 epoxy resin is a variant of the baseline 8552 resin and was designed for fiber placement. Compared to 8552, the 8552-1 variant demonstrates a lower tack; facilitating movement through the fiber placement head.

The IM7/8552-1 prepreg material was ordered to Hexcel's internal specification HS-AD-971B and meets the following:

- Fiber Areal Weight (FAW): 190 gsm
- Resin Content: 33 ± 2%
- IM7 12K –G sized fiber.

The parent tape was fabricated at Hexcel Corp, Salt Lake City, UT, and slit at Web Industries, Atlanta, GA. The slit tape width specifications included a ¼" wide tape provided to NASA Langley for fabrication of the three panels.

3.2 Lay-up design and preparation

Automated Fiber Placement lay-up begins with Computer aided Design software and Composite Programming Software to read CAD surfaces and ply boundary information to add material, filling the plies according to the user-specified manufacturing standards and requirements. Layup paths are then linked together to form specific layup sequences and output as NC programs for the automated layup machine. The panel layups were first programmed using the CGTech Vericut for Composites Programming (VCP) software, as shown in Figure 9.

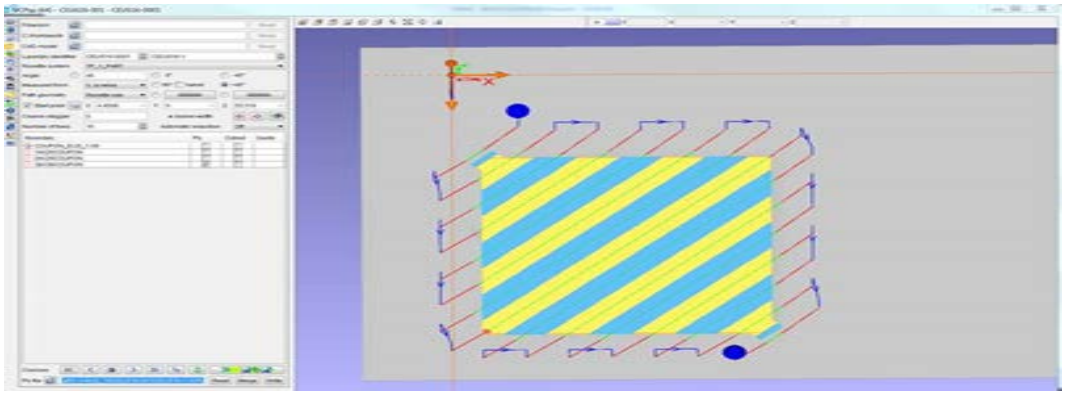

Figures 9: CGTech Vericut for Composites Programming (VCP) software.

The key difference between the three panels during the programming phase were the stacking sequence between the pristine quasi-isotropic and unidirectional panel.

Additional software is used to simulate the work environment for automated fiber placement manufacturing. Through CAD models and NC programs, this program simulates the sequence of NC programs on a virtual machine, including head changes, probing, knife cutting, and more. Material is applied to the layup form via NC program instructions in a virtual CNC simulation environment. The simulated material applied to the form can be measured and inspected for stack thickness, ply offset, ply angle, and other manufacturing priorities to ensure the NC program follows manufacturing standards and requirements.

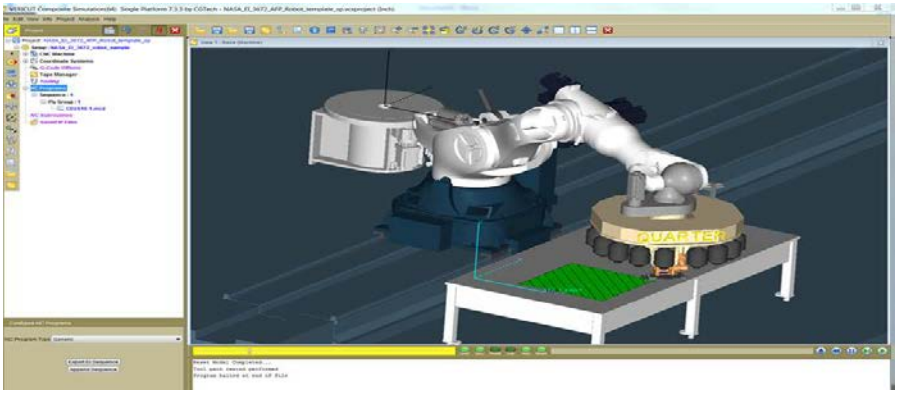

Figure 10: CGTech Vericut for Composites Simulation.

A report showing simulation results and statistical information can be automatically created to enable the user to predict or analyze the lay-up and mitigate risk to improve the user's process. The nc path generated is then tested virtually prior to running on the ISAAC hardware using the CGTech Vericut for Composites Simulation (VCS) software as shown in figure 10.

3.3 Lay-up fabrication

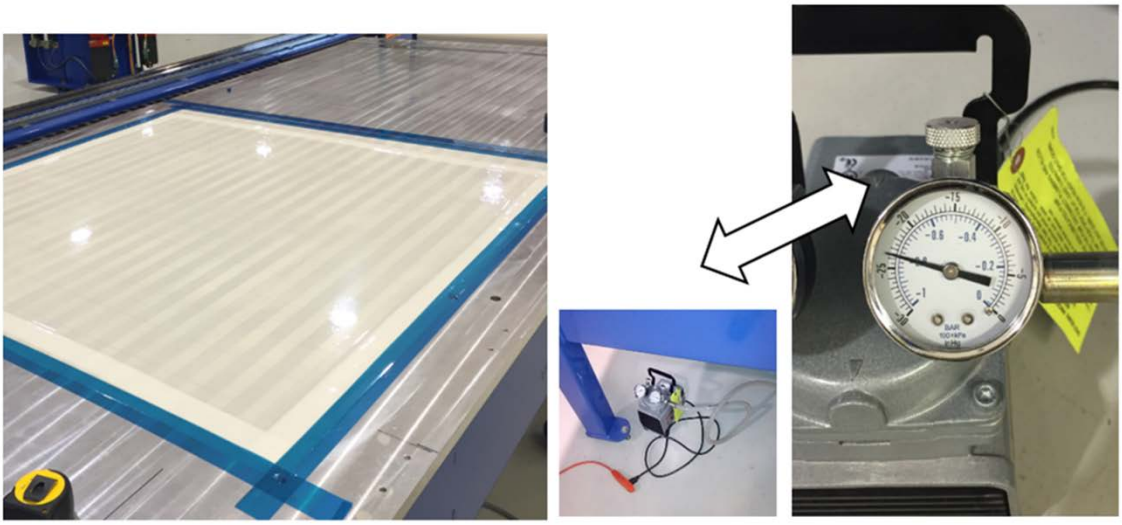

Figure 11: Lay-up preparation

Next, begins the actual layup manufacturing process where the users place the material on the robot and run the layup through CNC software. To begin the layup, the surface must be prepped in order to ensure the panel is smooth and free of foreign materials that could be integrated into the part. This is done by using mylar and a vacuum as shown in figure 11.

Figure 12: AFP Lay up example

After surface preparation, the layup begins by uploading the program onto the robot and performing a dry run to ensure the machine doesn't crash or interfere with any other fixtures as a verification step along with laying up the defects first to ensure that they are at the right locations.

The AFP end effector feeds the tows in front of a heat source and under a consolidation device (roller) and cut. The heat will make the thermoset tape tackier, allowing the incoming material to be stuck onto the substrate when pressed down by the consolidation device. At the end of each course, any tows in process are cut and the robot moves to the start of the next course when told to do so by the program controlling the process. The process is repeated course-by-course until each ply is complete and ply-by-ply until the final part geometry is achieved. For the quasi-isotropic panel and unidirectional panel, different programs with their stacking sequences were uploaded onto the machine.

3.4 Defect Panel design and fabrication

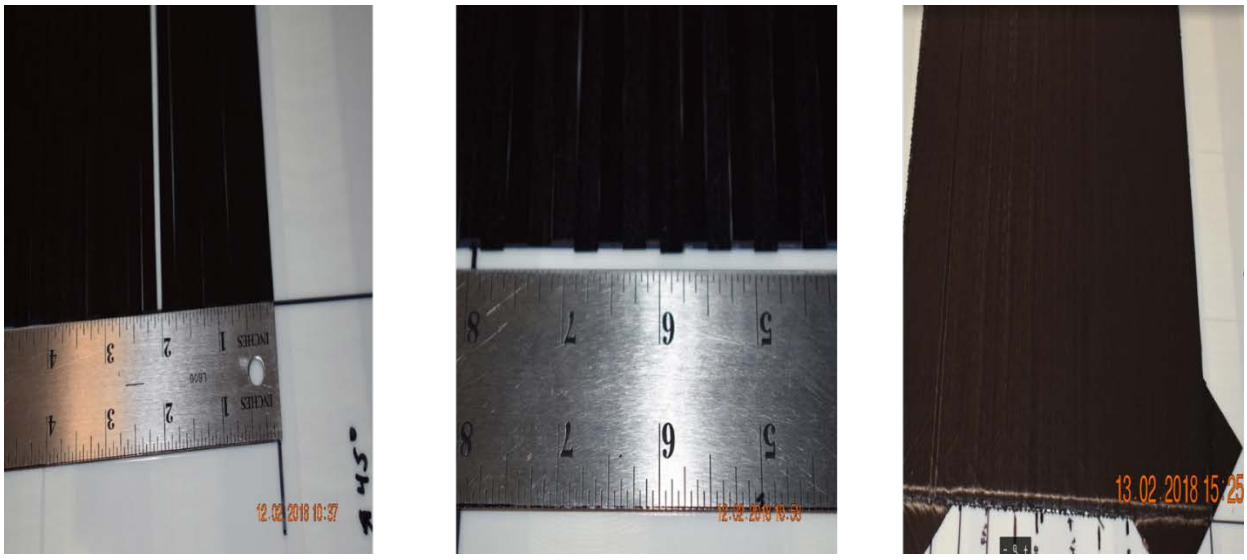

Figure 13 Defect Verification Gap, Lap, Fold (Right to Left)

When programing the gap and overlap features in the quasi-isotropic defect panel, a measurement of 0.1 inch was used for each defect. The defects were also programmed in the near bottom surface (ply2), the midplane surface (ply 10), and the near top surface (ply 23) in the zero degree direction. The fold defect was not programmed and will be mentioned in the actual lay-up.

For the defect panel, the gap and overlap were programmed, but the fold defect was manually placed in plys 2,10 and 23 at certain locations because of the software's inability to place this type of defect consistently. This defect was made by removing the tows at certain locations along the zero degree direction and folding the tow in half, then placing the folded tow in the middle of the tow. After each ply was done, researchers and technicians performed a visual inspection and signed off to continue to the next ply until the parts were complete.

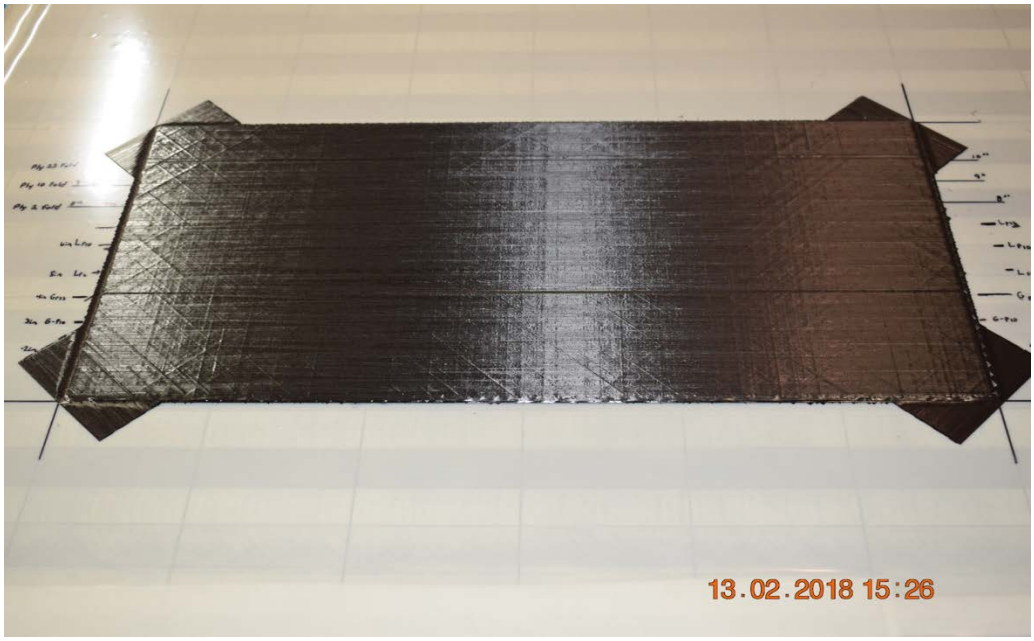

Figure 14: Defect panel overview

3.5 Autoclave processing, analysis and sample preparation

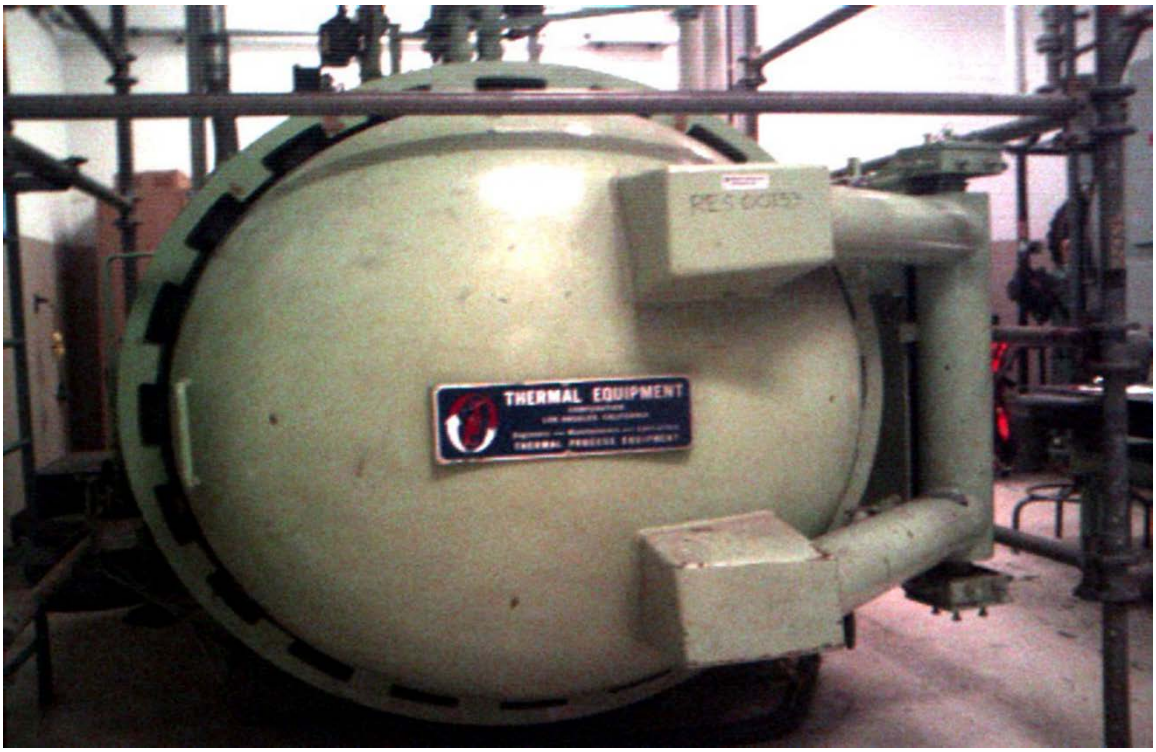

Figure 15: Autoclave used for processing

Generally, after layup, manufacturers use an additional process involving the prepreg carbon fiber for cutting, vacuum bagging and curing by an auto clave. The purpose of this process is to fabricate test panels for use in material qualification, equivalency, and acceptance testing. After layup on ISAAC, the panels were then cured at NASA Langley using the cure cycle specified by the referenced processing document.

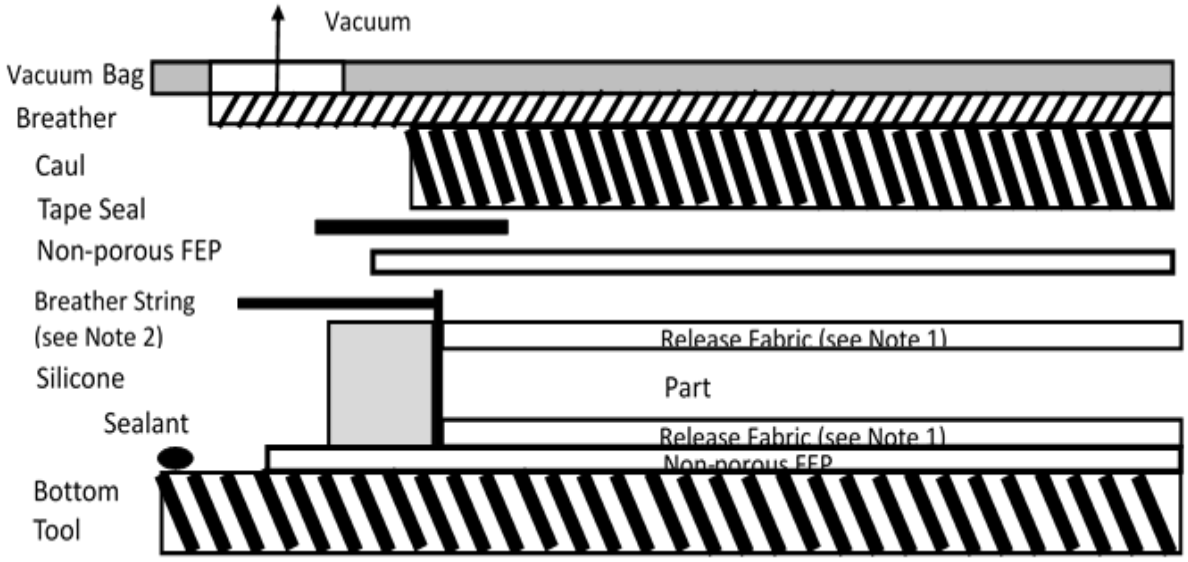

Figure 16: Composite bagging overview

Figure 16 details the bagging arrangement used to manufacture equivalency test panels. The cure cycle outlined below was followed, again to mirror NCAMP processing conditions. This cure profile, identified as 'baseline/medium cure cycle (M)', varied from the vendor recommended cycle.

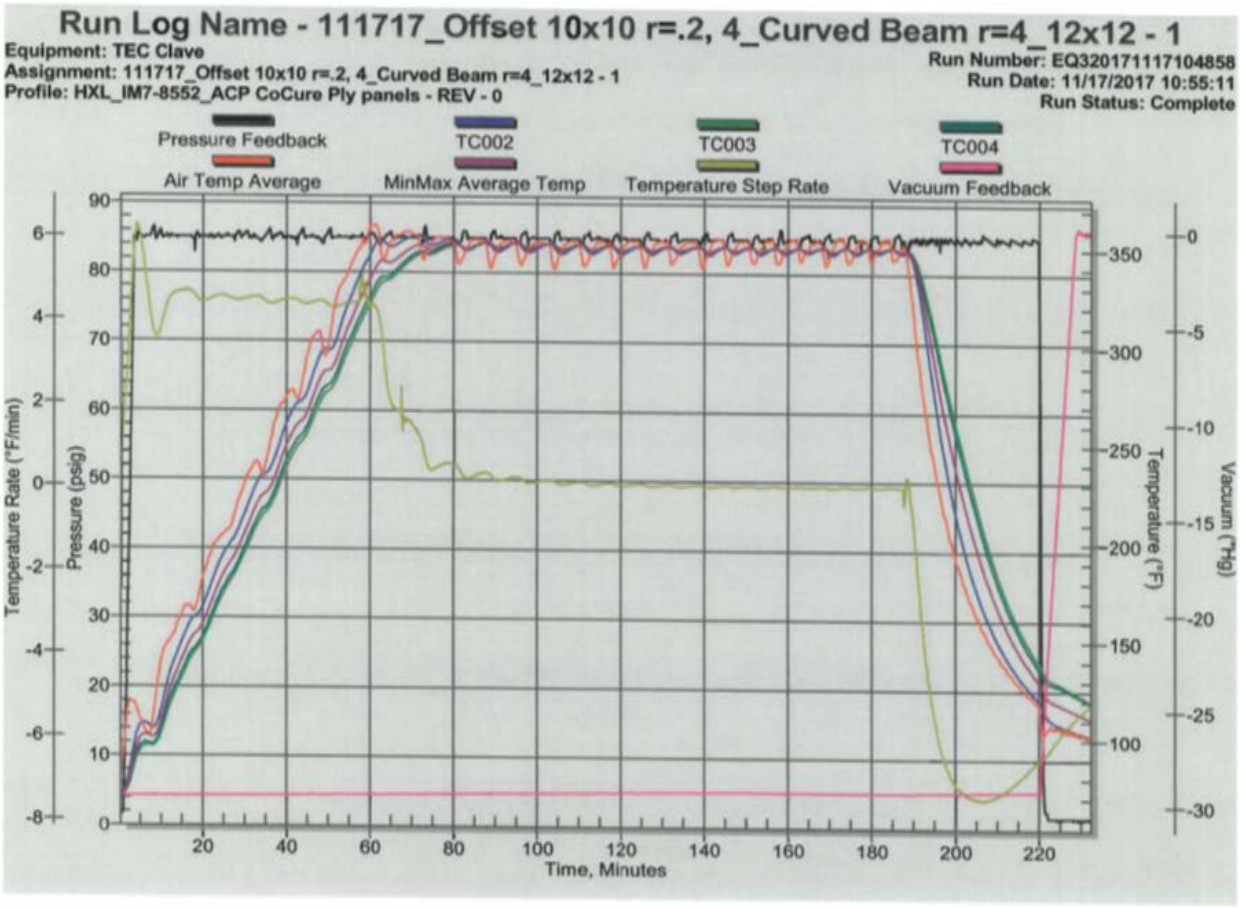

Figure 17: Autoclave cure cycle representative for all panels

The steps for the Baseline/Medium Cure Cycle are listed below. l Technicians must check the vacuum bag integrity prior to starting the cure cycle. The leak rate should not exceed 5 in. Hg in 5 minutes. All temperatures are part temperatures and are based on leading thermocouple, except step e. is based on lagging thermocouple.

a. Pull vacuum (min. 22 in. Hg).

b. Heat at 2°F/min to 355 ±10°F and ramp autoclave pressure to 100 psig.

c. Before temperature reaches 140°F and when autoclave pressure is 20 ±10 psig, vent vacuum bag to atmosphere.

d. From 325°F to 355 ±10°F a minimum heat up rate of 0.3 °F/min is acceptable.

e. Hold 355 ±10°F for 120 +60/-0 min.

f. Cool down rates from cure temperature to 150°F shall be no more than 10°F/minute.

g. Release autoclave pressure when lagging thermocouple is below 150°F or minimum 1 hour into cool down, whichever occurs sooner.

h. Remove from autoclave when autoclave temperature is less than 120°F.

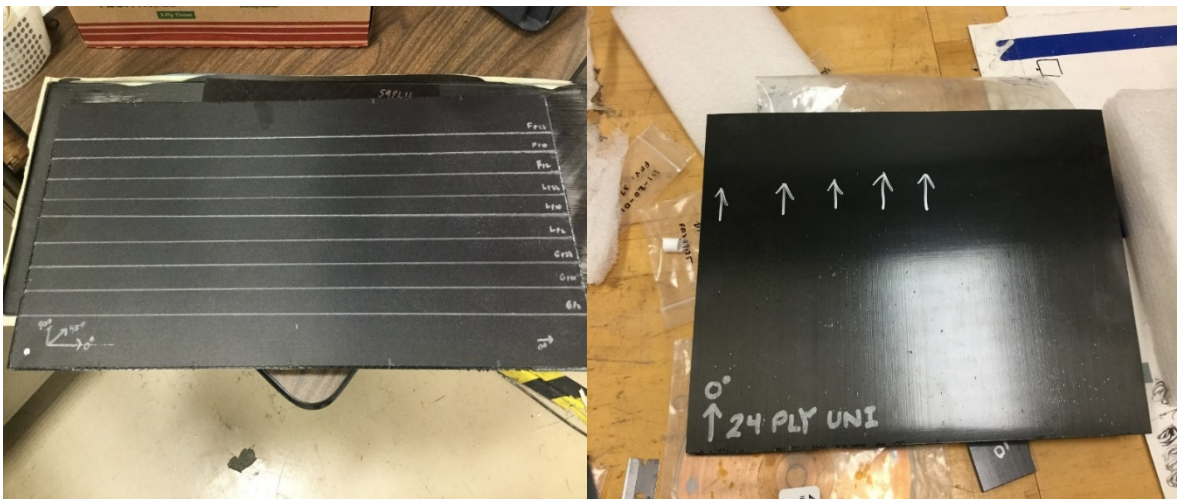

Figure 18: Post processing Defect panel (left) Unidirectional panel (right)

After processing as shown in figure 18, the Quasi-isotropic and Unidirectional panels were then cut up, using a diamond tip saw, into approximately 6 x 6 x 6 mm cube samples. However, for the defect panel, Non-Destructive Evaluation such as a C-scan was conducted to verify that the defects were still in the same locations after autoclave processing.

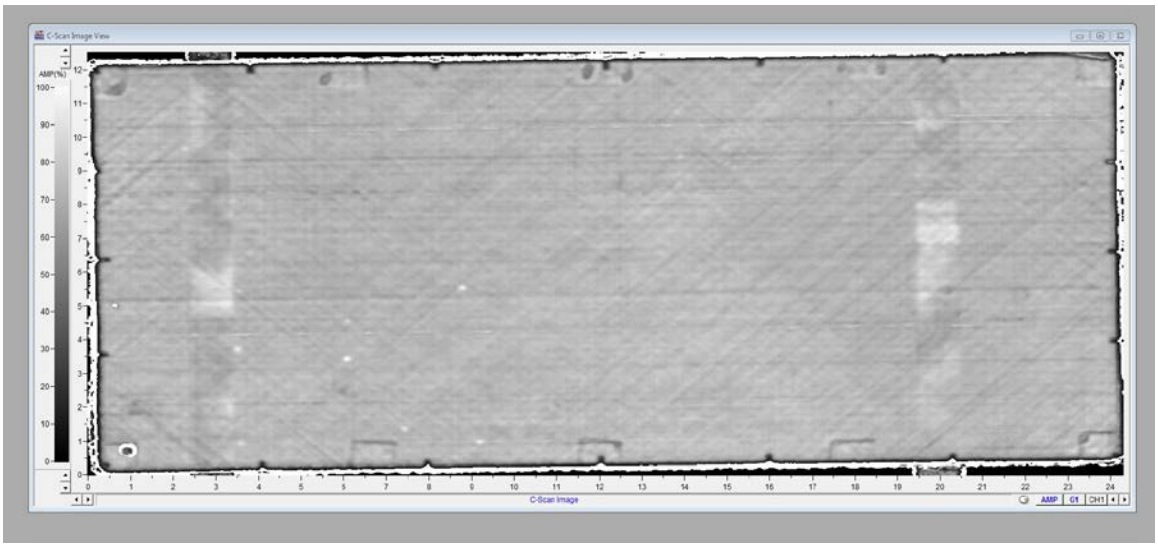

Figure 19: C-scan for defect panel

Figure 19 shows the c-scan results for the defect quasi-isotropic panels. The two vertical bar lines across the panel are the structures holding the panel in place for analysis. In figure 20, the red lines shown indicate certain anomalies. These anomalies at those locations are where certain defects were placed. The lower portion of the panel contains the gap defects, the middle containing the overlap and the upper portion containing the folds, with their sections divided into different through thicknesses.

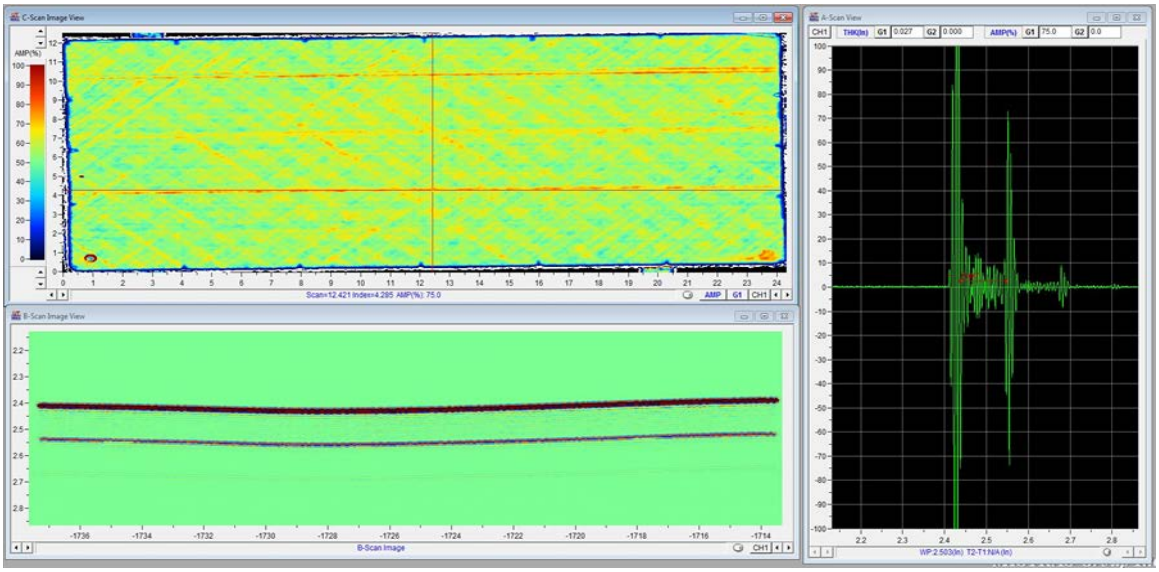

Figure 20: A-scan, B-scan, and C-scan for defect verification

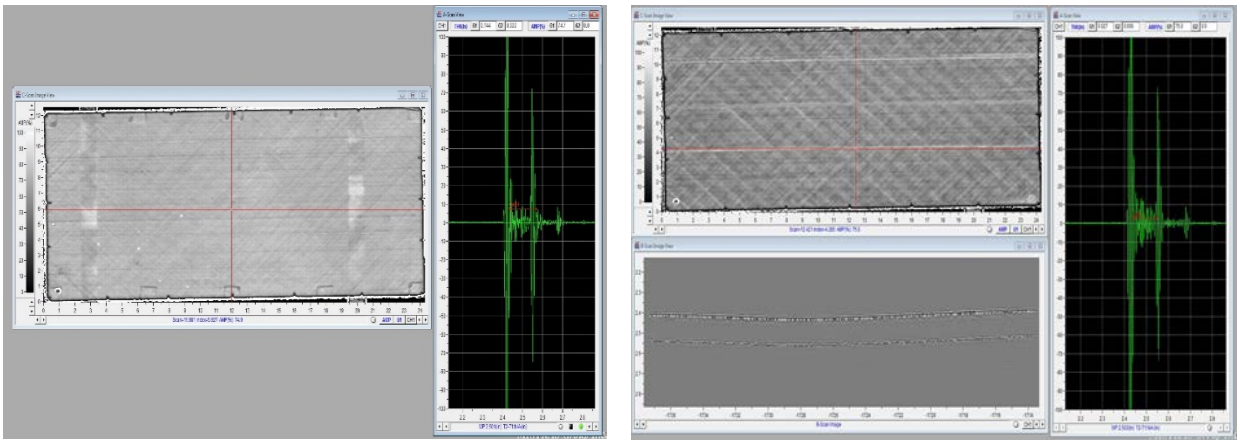

Figure 21: A-scan, B-scan, and C-scan for defect verification

The A-scan screen indicates the signal of any anomalies (defects). The two spikes from the left to right are with respect to the top viewpoint to the bottom of the panel. The small signal in the middle indicates the presence of a defect at certain locations where the large red crosshair is located. Figure 21 shows the signal of an overlap defect while figure 20 shows a defect in the gap region. The B-scans can indicate any anomalies from the front and back viewpoints of the panel. The scan verifies the visual inspection during fabrication that the embedded defects were placed in their respective positions and locations.

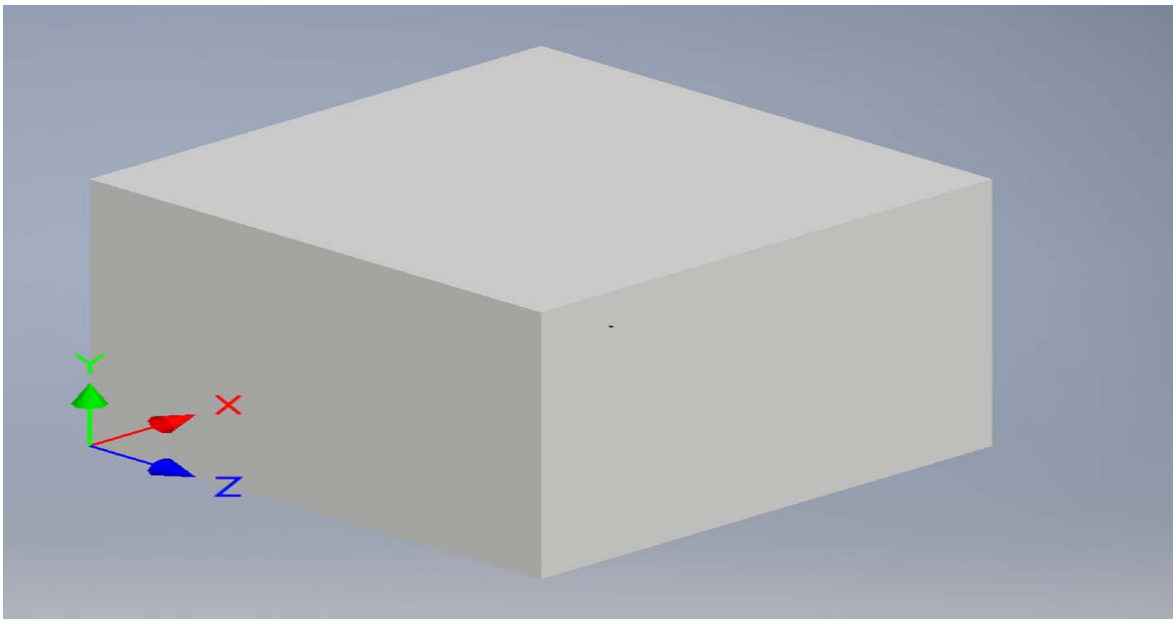

Figure 22: Cube sample design with coordinate layout

Afterwards, as shown in figure 22, the panels were cut up, using a diamond tip saw, into approximately 6 x 6 x 6 mm cube samples. Note that only the defect panel has undergone post processing analysis. During sample preparation, the samples are weighed for their mass and marked with an arrow along the 0° direction for consistency and identification in order to test for the different directions. The following directions were identified for testing purposes:

X- Direction along the fibers

Y- Transverse Direction

Z- Through the thickness

3.6 Quasi-static testing

After sample preparation the samples were tested using a universal testing machine. Quasi-static means that at a given instant in time we can assume the problem is static. This testing technique uses cyclic loading and displacement on the structure to give the researcher insight regarding the behavior of a structure in the post yielding regime. This assumption works well when inertial effects are very low and therefore negligible. Around five samples from each direction were tested at a rate of 0.5 $mm*s^{-1}$.

3.7 Dynamic testing

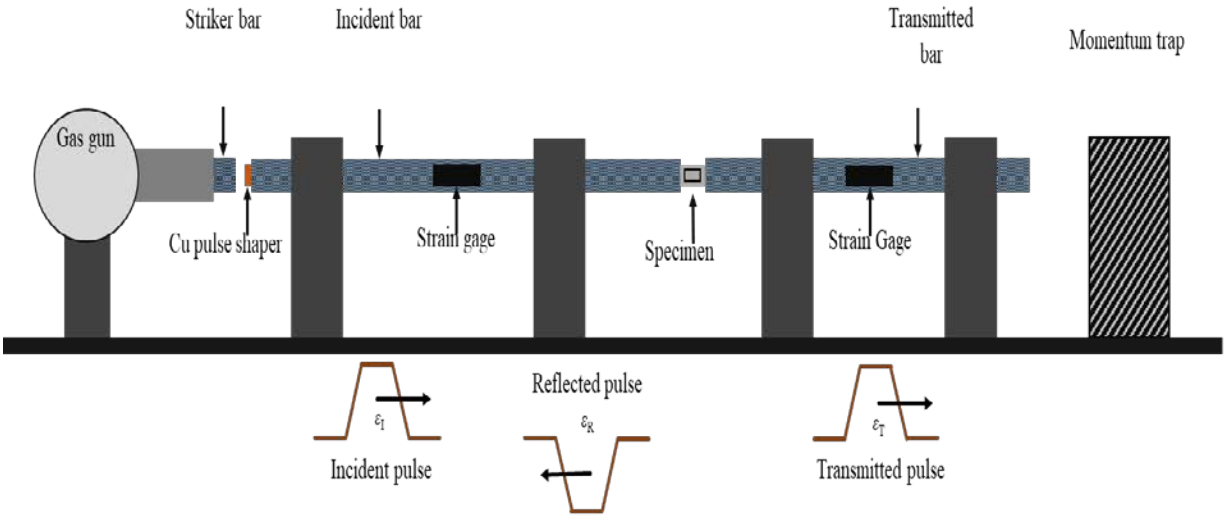

Figure 33: Split Hopkinson Pressure Bar layout

The SHPB comprises a striker bar, an incident bar, and a transmitted bar as shown in figure 23. A specimen is placed between the incident and transmitted bars, and the striker bar is propelled at a specified velocity, hitting the incident bar and causing compression on the specimen lodged between the two previously mentioned bars; strain gages are implemented to collect the data. The theory for SHPB is based on classical mechanics of elastic wave propagation in the bars and on the principle of superposition of waves. In elastic wave

propagation theory, stress, strain and particle velocity are caused due to pressure waves (here compressive) proportional to each other. Hence, knowledge of a single pressure wave at any cross-section of the bars enables us to calculate the wave nature at any other cross-section. A list of the measurement parts used in the SHPB apparatus is given.

Using the knowledge of incident wave and reflected wave at any cross-section and through the principle of superposition, stress, strain and particle velocity can be calculated. Here the stress, strain and particle velocity are simply the sum of those related to the incident wave and reflected wave, which are in opposite directions (Zhao and Gary, 1996).

CHAPTER 4

RESULTS

This chapter discusses the results from the quasi-static and dynamic test. After the tests were performed the signals were processed using Matlab software to calculate the peak strength of each sample. Other measurements such as the strain rate and strain were taken, but due to the unreliability of the data, they were removed from this thesis.

4.1 Pristine Quasi-isotropic and Unidirectional

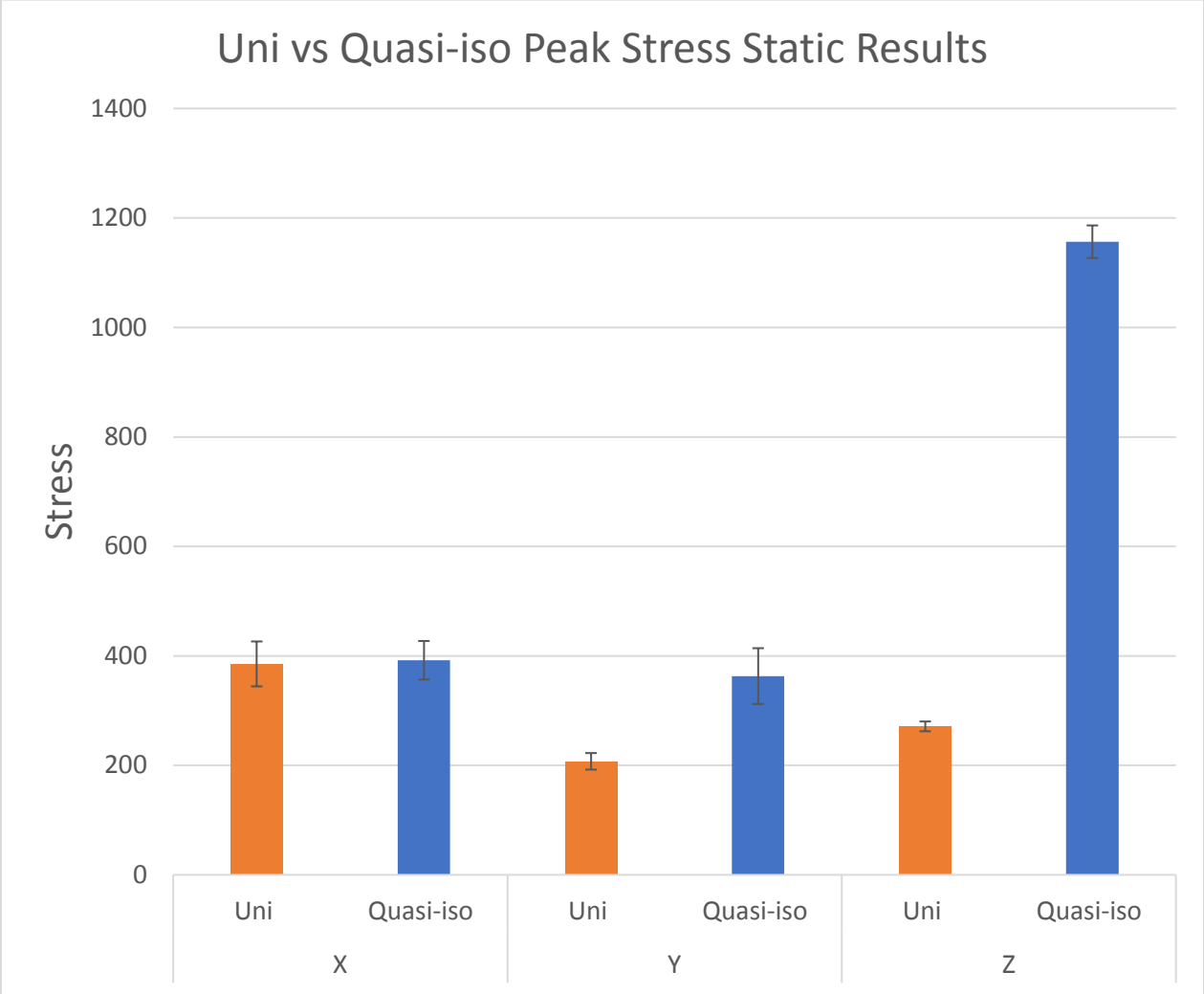

Figure 24: Unidirectional vs Quasi-isotropic panel peak quasi-static stress results

From figure 24, the samples from each direction were gathered and averaged to give an overall result for the pristine quasi-isotropic panel and unidirectional panel under quasi-static testing conditions. From the overall average, the standard deviation was calculated and added into the bar graph. The results from the pristine quasi-isotropic panel will later be used as a baseline for the results from the defect panels.

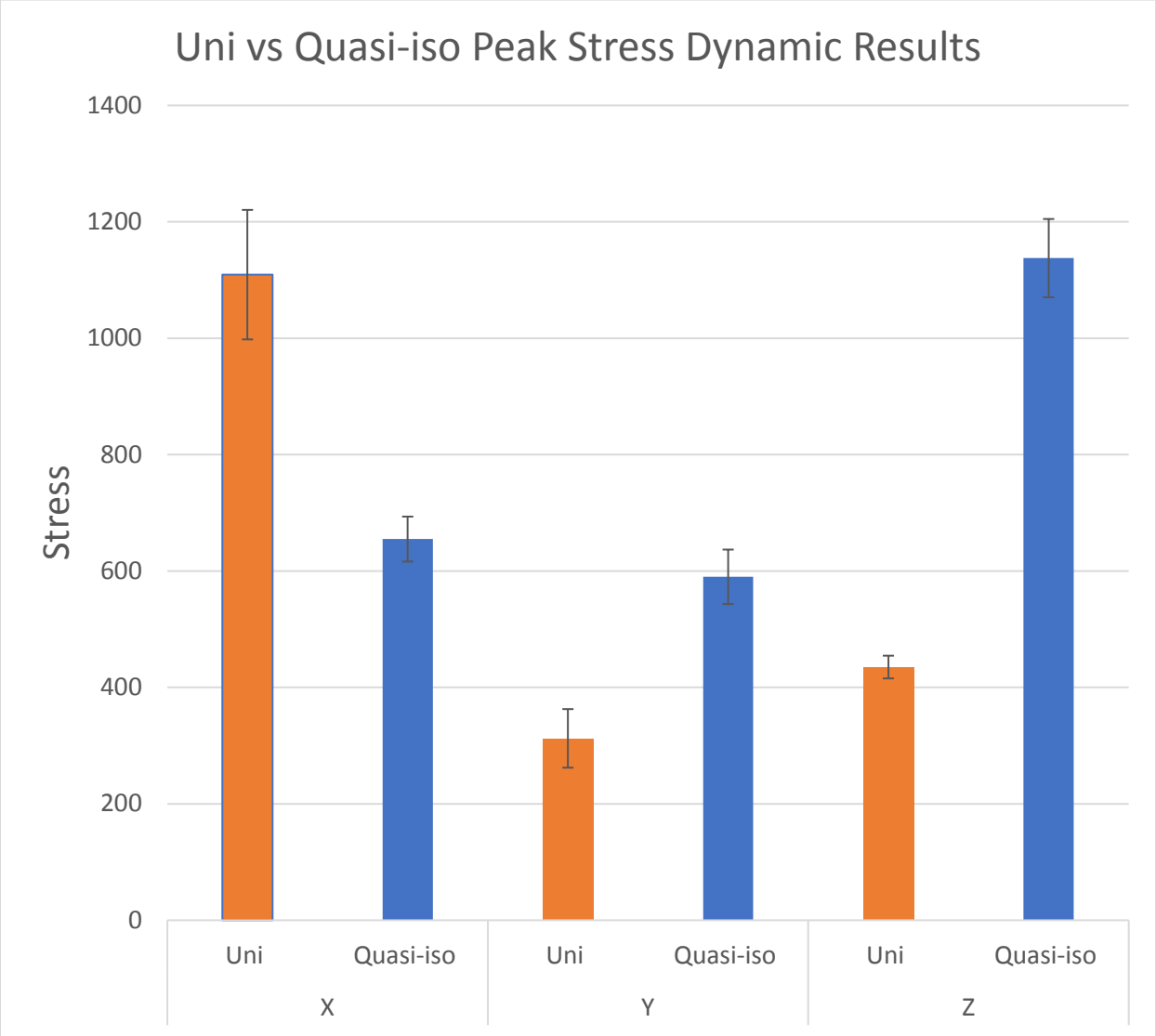

Figure 25: Unidirectional vs Quasi-isotropic panel dynamic peak stress results

From figure 25, the samples from each direction were gathered and averaged to give an overall result for the pristine quasi-isotropic panel and unidirectional panel under dynamic testing conditions. From the overall average, the standard deviation was calculated and added into the bar graph. The results from the pristine quasi-isotropic panel will later be used as a baseline for the results from the defect panels.

4.2 Quasi-static Results for the defect panels

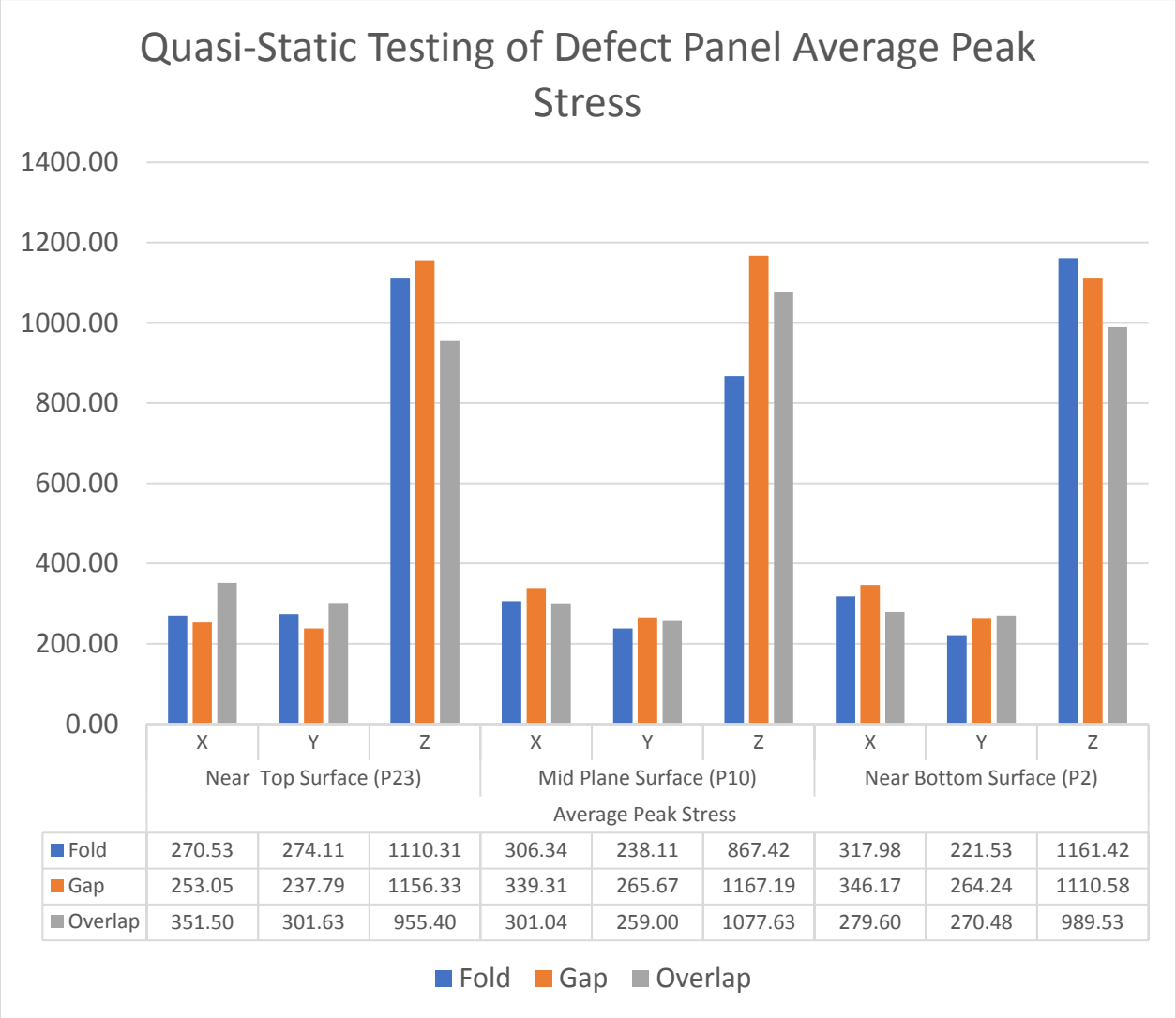

Figure 26: Overall Quasi-static Defect Panel Results

Figure 26, shows the results of the gap, overlap, and fold defects in the x, y, and z directions under quasi-static conditions. A total of 5 samples were tested for each defect in each direction, in each surface plane. The results were then averaged to give the results shown. Figures 27, 28, and 29 show the defects compared to their quasi-isotropic baseline listed above in

figure 26. In Figure Z in the z direction in ply 10, the bar is red because the result was higher that the baseline.

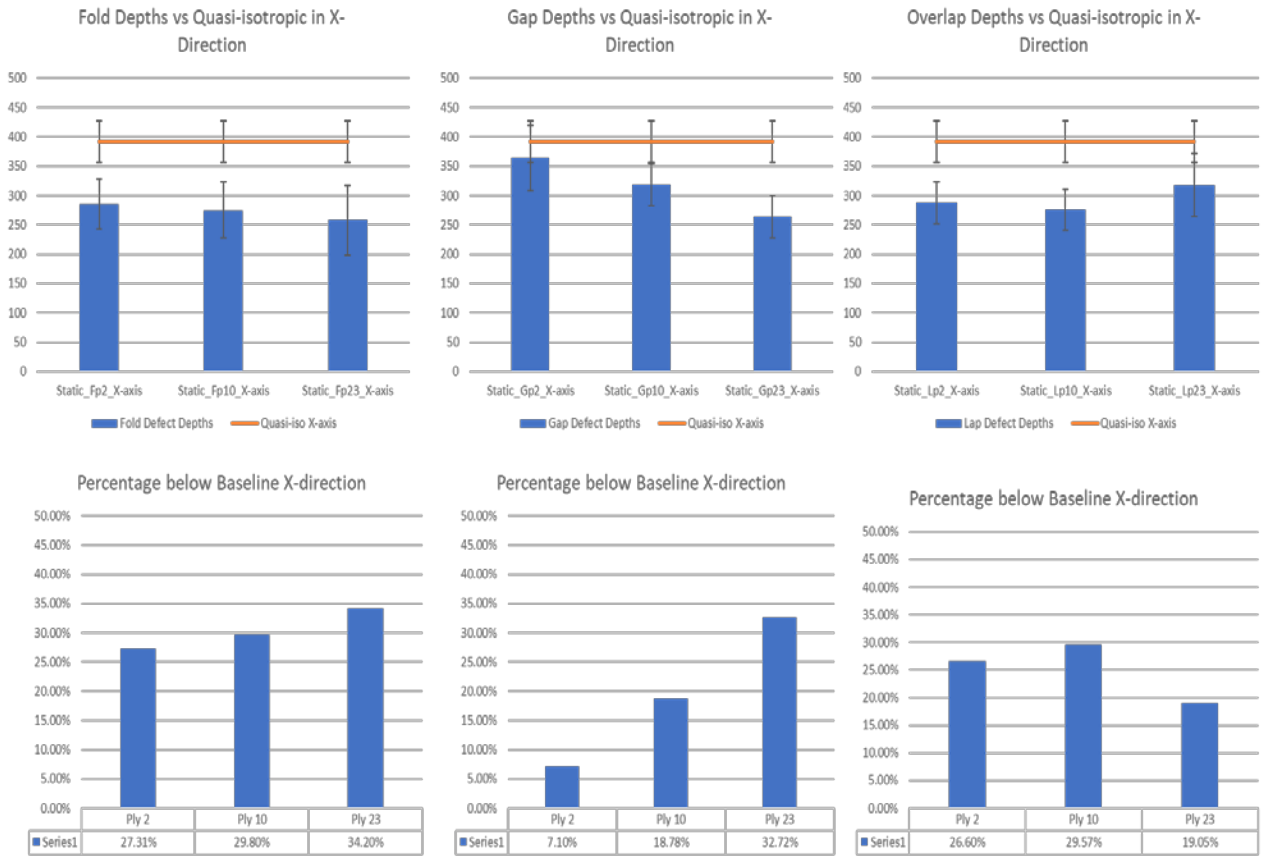

Figure 27: Defect Depth vs Quasi-isotropic Baseline with Normalized results in the X-Direction

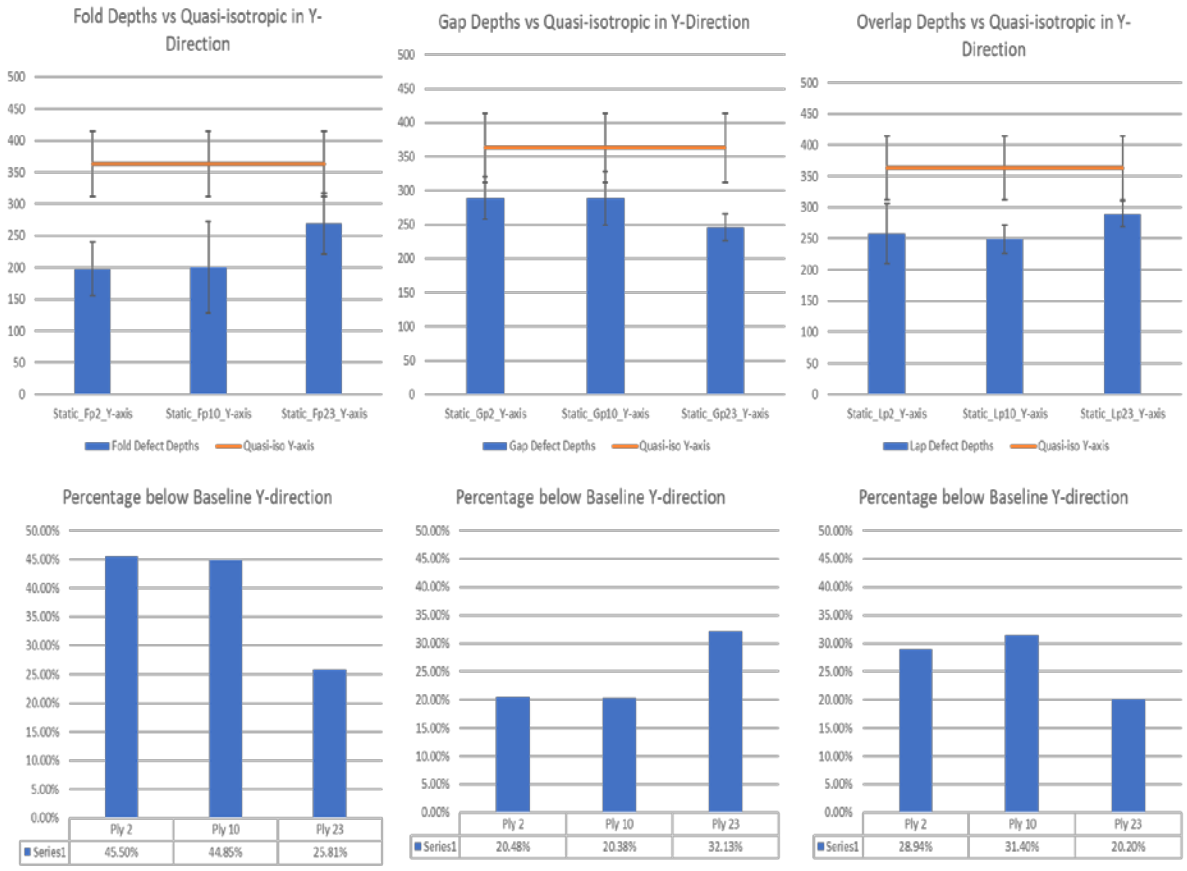

Figure 28: Defect Depth vs Quasi-isotropic Baseline with Normalized results in the Y-Direction

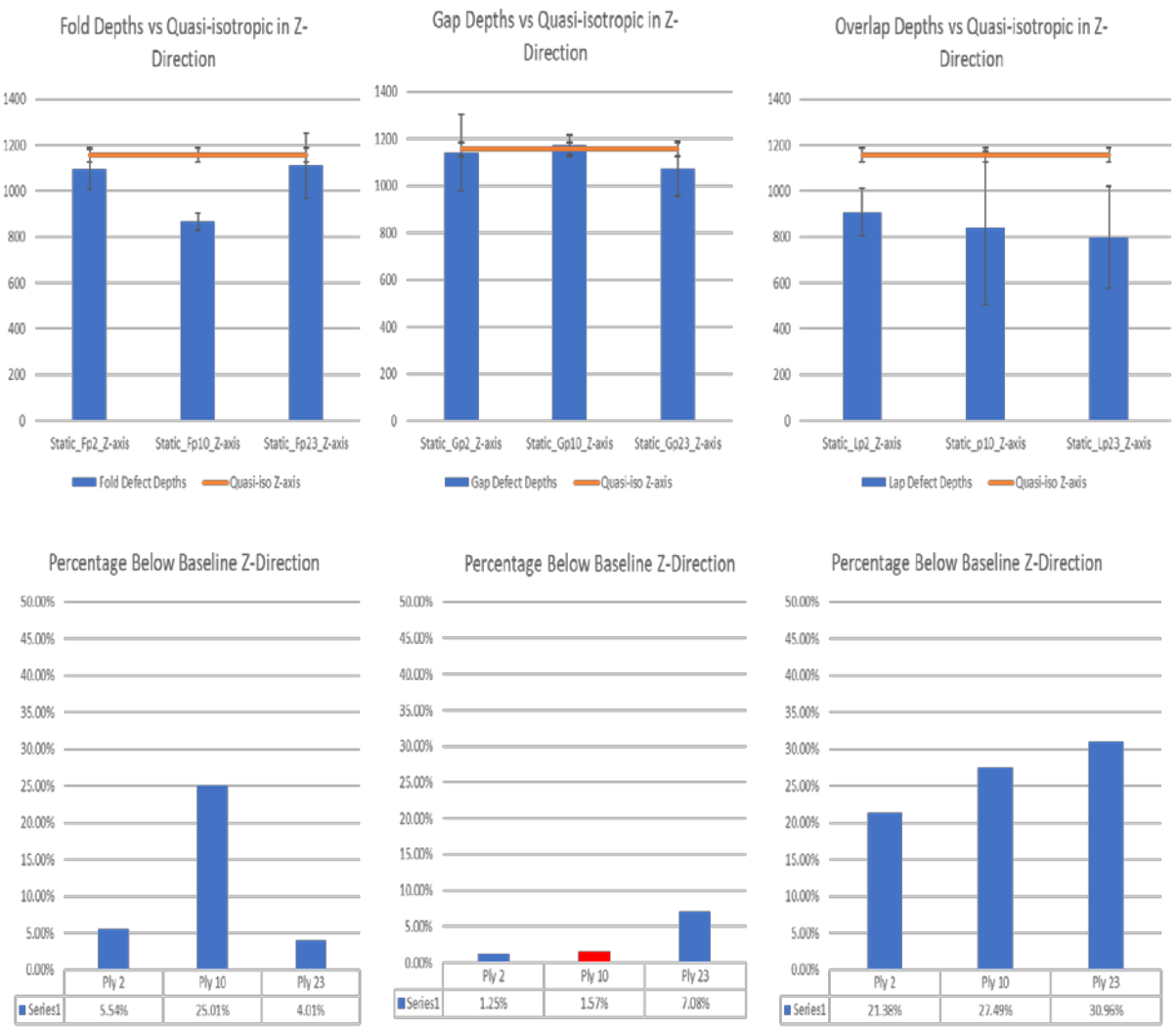

Figure 29: Defect Depth vs Quasi-isotropic Baseline with Normalized results in the Z-Direction

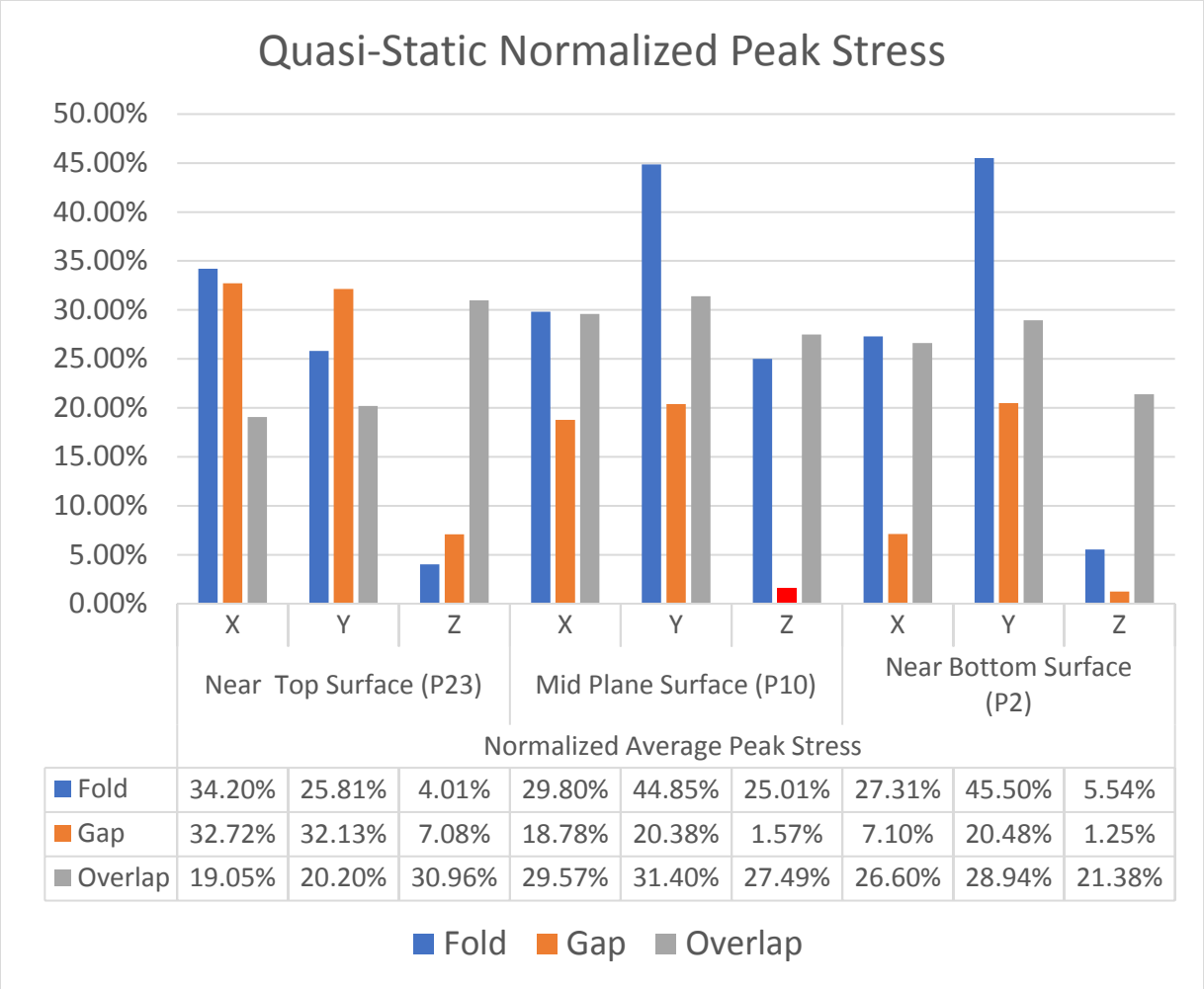

Figure 30: Overall Quasi-static Normalized Defect Panel Results

Figure 30 shows the normalized averaged results of the gap, overlap, and fold defects in the x, y, and z directions under quasi-static conditions. In Figure Z in the z direction in ply 10, the bar is red because the result was higher than the baseline.

4.3 Dynamic Results for the defect panel

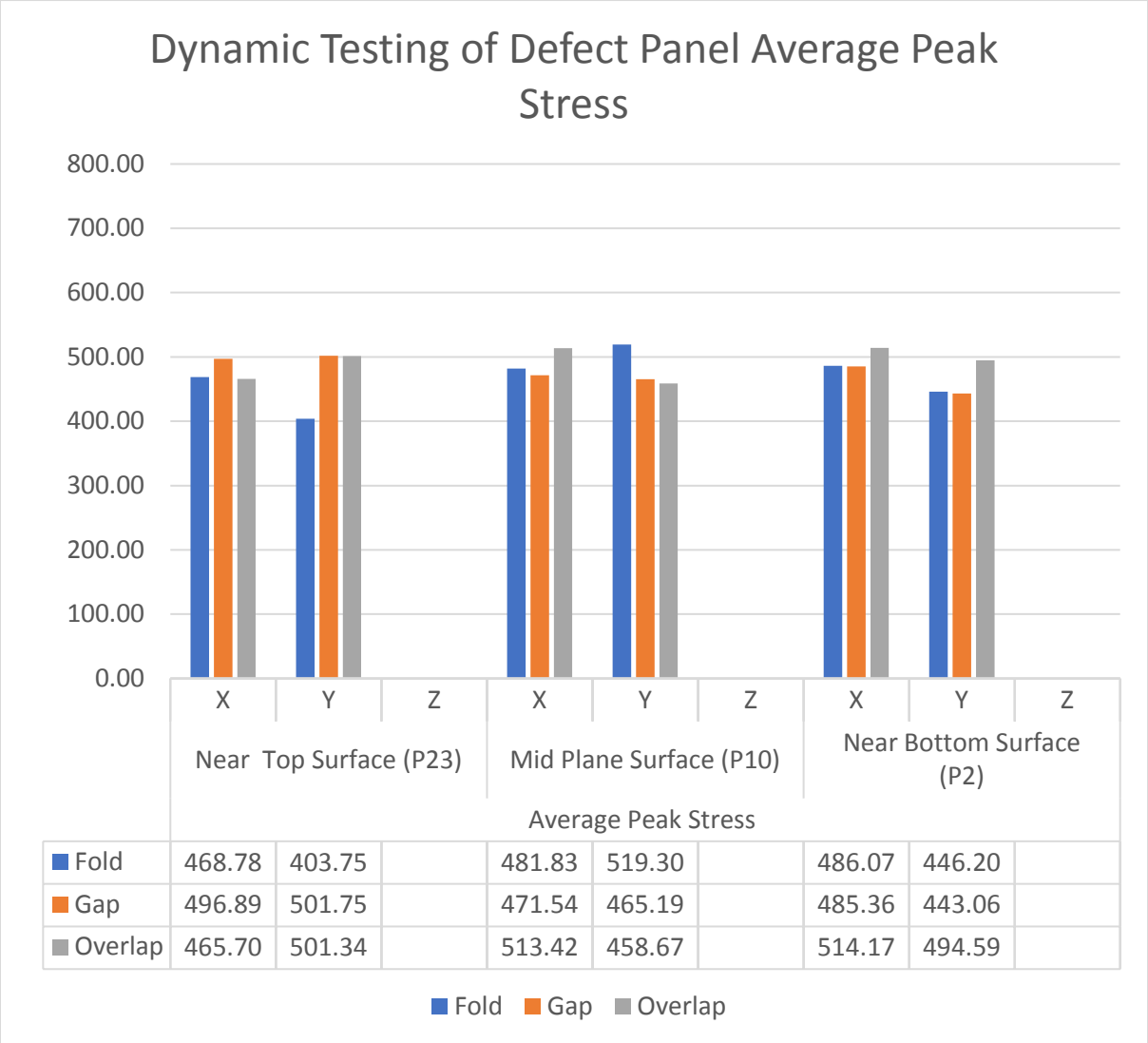

Figure 31: Overall Dynamic Defect Panel Results

Figure 31 shows the results of the gap, overlap, and fold defects in the x and y directions under dynamic conditions. A total of 5 samples were tested for each defect in each direction, in each surface plane. The results were then averaged to give the results shown. Figures 32 and 33 show the defects compared to their baseline dynamic listed above in figure 32. The Z direction was not tested due to time constraints, leaving a questionable result for through thickness.

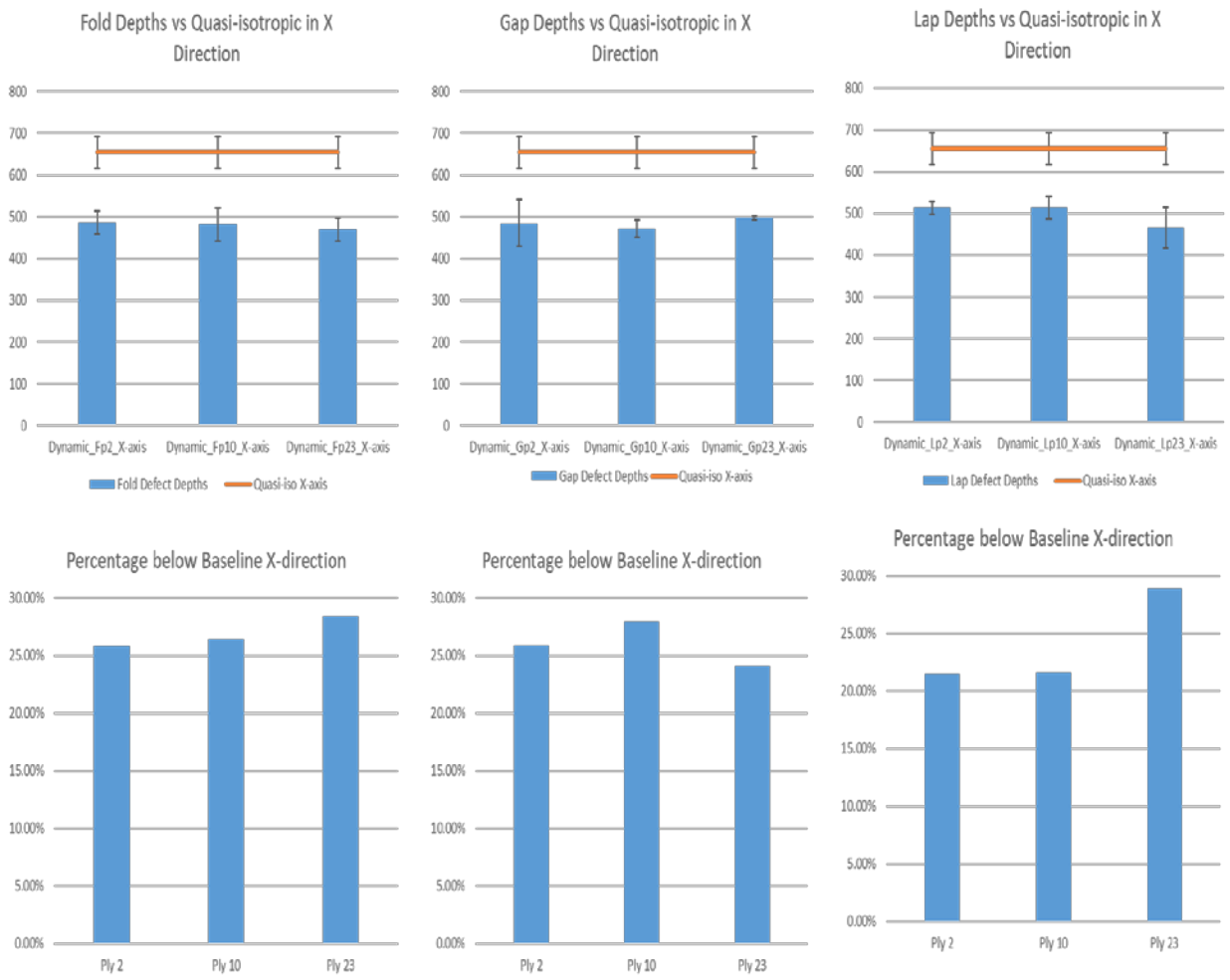

Figure 32: Defect Depth vs Quasi-isotropic Baseline with Normalized results in the X-Direction

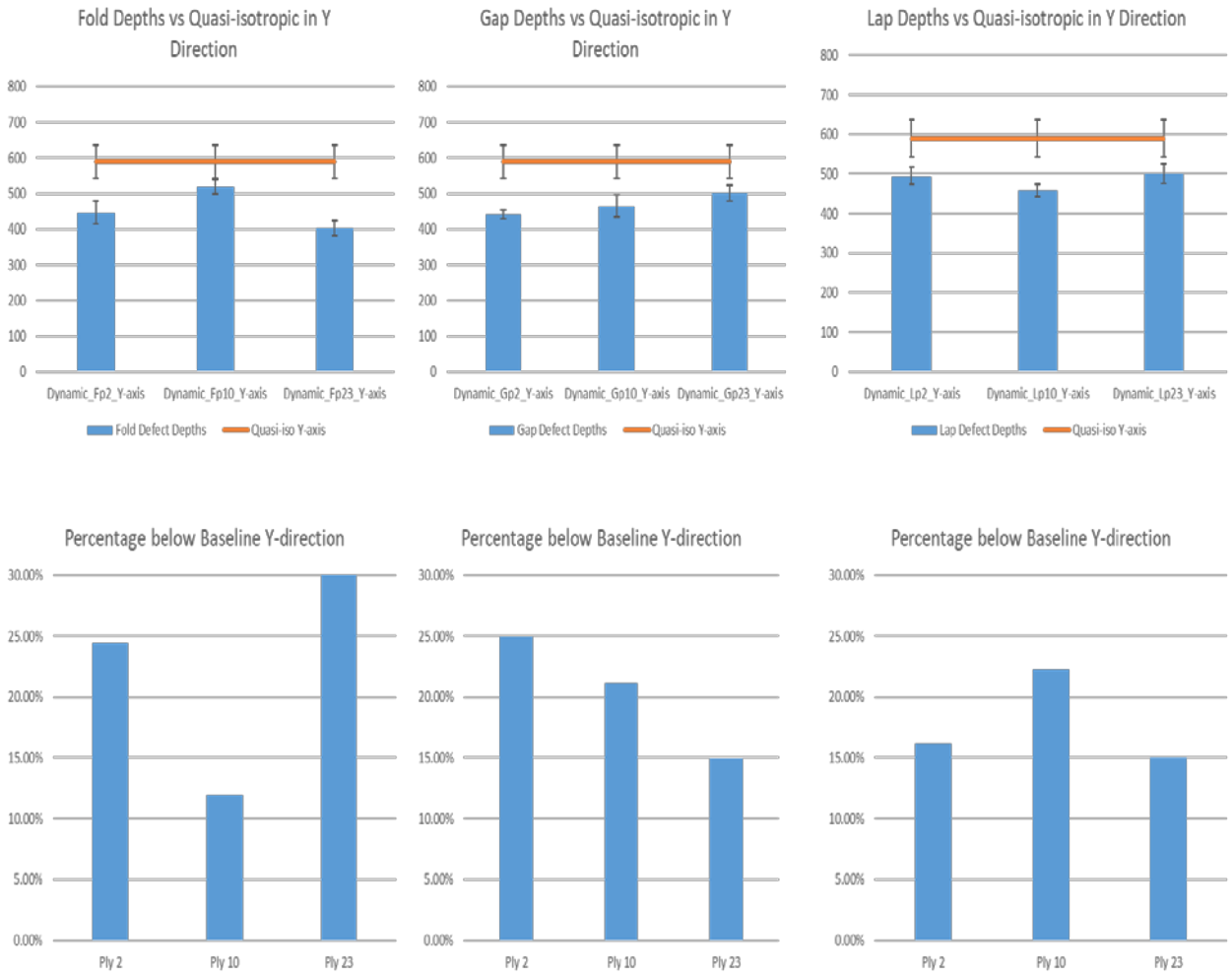

Figure 33: Defect Depth vs Quasi-isotropic Baseline with Normalized results in the Y-Direction

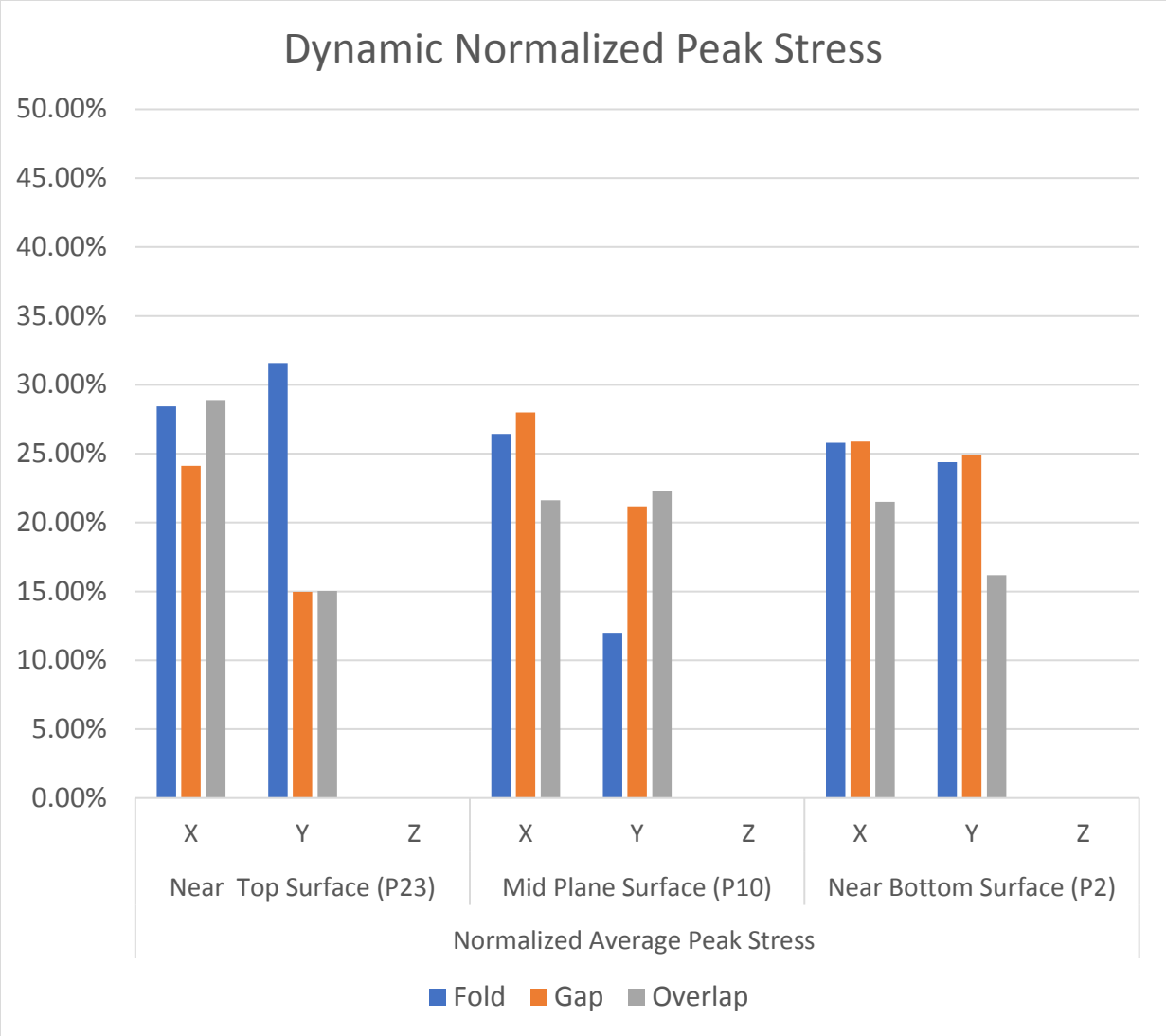

Figure 34: Overall Dynamic Normalized Defect Panel Results

Figure 34 shows the normalized averaged results of the gap, overlap, and fold defects in the x, y, and z directions under dynamic testing conditions.

4.4 Overall static vs dynamic results

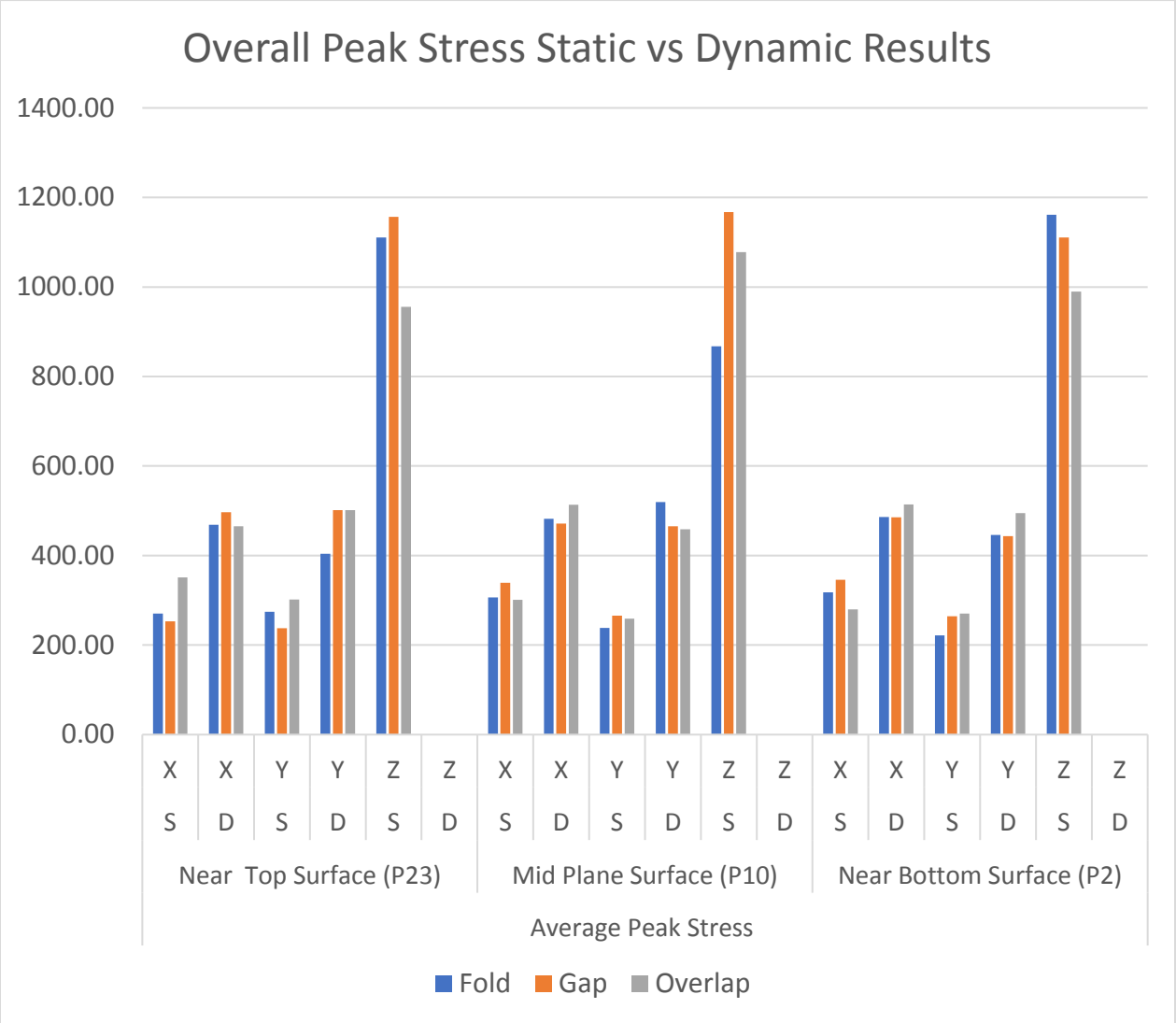

Figure 35: Overall Static vs Dynamic Peak Stress Defect Panel Results

Figure 35 shows the overall results comparing the quasi-static and dynamic total averaged strengths for the gap, overlap, and fold defects in the x, y, and z directions in the near bottom, mid plane, and near top surface planes.

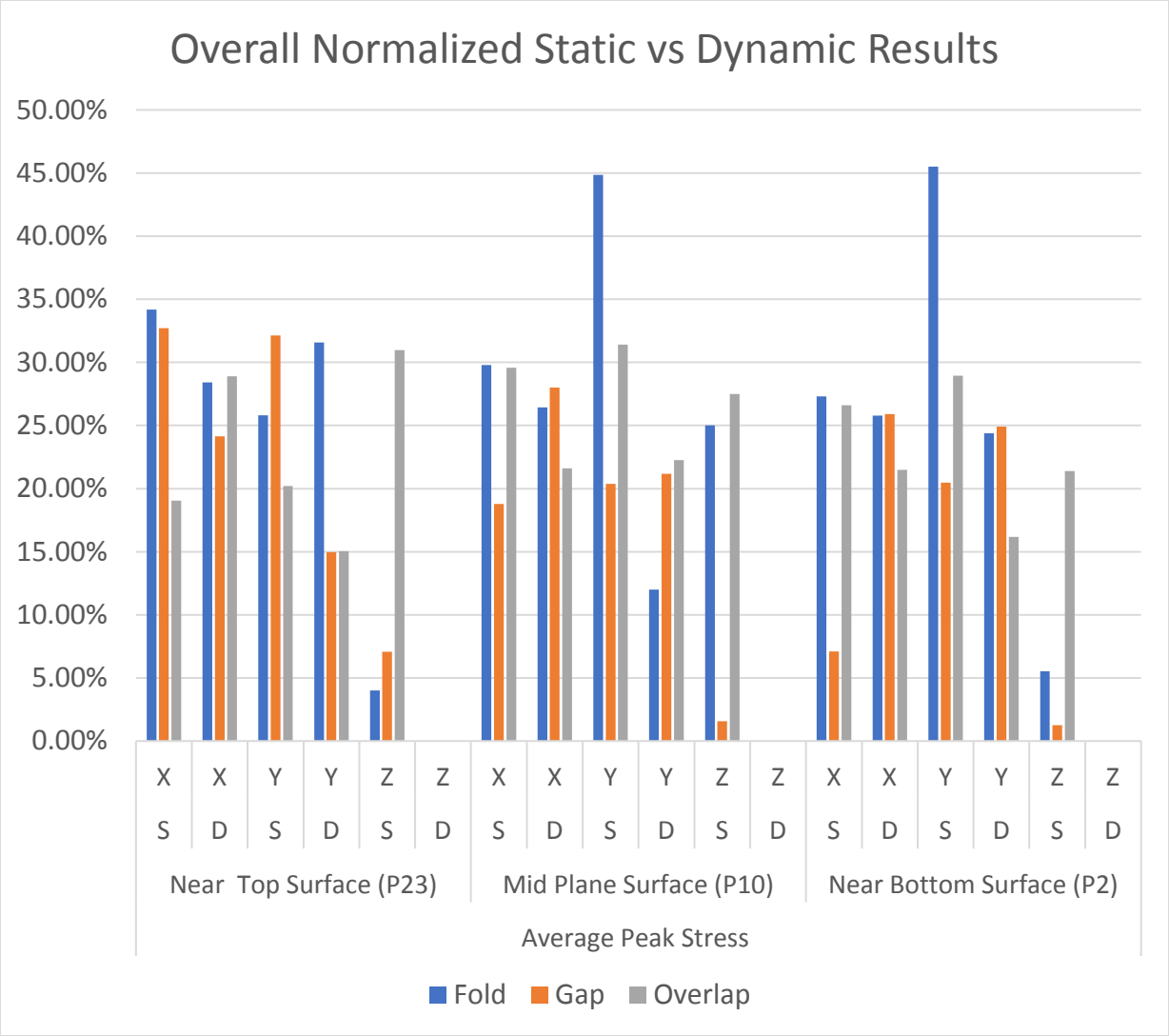

Figure 36: Overall Normalized Static vs Dynamic Peak Stress Defect Panel Results

Figure 36 shows the overall normalized results comparing the quasi-static and dynamic total averaged strengths for the gap, overlap, and fold defects in the x, y, and z directions in the near bottom, mid plane, and near top surface planes.

CHAPTER 5

CONCLUSION

5.1 Conclusions

For the quasi-static and unidirectional testing results, an observation is that the Y-direction (unidirectional samples) tested under dynamic experimentation is around half of the strength for the Quasi-isotropic samples in the transverse direction. Though the thickness (Z-direction) strength is higher than the transverse direction for the Quasi-isotropic samples, under both static and dynamic testing conditions, the strength of the Z-direction unidirectional samples are higher than the Y-direction in both static and dynamic testing conditions. There are similar trends of increased strength with strain rate observed with the quasi-isotropic samples but not as prominent as the X-direction. The same trend is observed for the dynamic testing results. For the quasi-isotropic panel, the X and Y directions have the same strength due to similarity of the stacking sequence in both sides.

After normalizing the data based on surface plane location, the data shows no significant deviation with the near bottom surface having an average twenty two percent, mid-plane surface having an average of twenty four percent, and near top surface having a twenty three percent reduction in strength. The fold defect has an overall reduction of strength by twenty six percent, followed by the overlap defect with an average of twenty four percent, and the gap defect by nineteen percent. Based on the results, the gap was the strongest of the defects, followed by the overlap, then the fold. Under the dynamic conditions in the X and Y direction, it appears to have a higher strength than in the static testing.

Direction wise, after normalizing the data, the Y-direction appears to have the greater reduction of strength by thirty percent compared to twenty five percent in the X-direction under

quasi static testing conditions. The defects along the X direction (along the fibers) may have caused the laminate to have a higher strength than the transverse direction. Under dynamic testing conditions, the results are inverse where in the X-direction there is a reduction of strength of twenty six percent and the Y-direction has a reduction of strength by twenty percent. The Z-direction has the least reduction of strength under quasi-static conditions with a reduction of strength of fourteen percent. Dynamic testing was not conducted for this thesis.

From the results of this study, the defects do show a significant reduction in strength. Based on the data achieved by conducting quasi-static and high-strain experiments, the roles of the controlled defects at different through-thickness locations show an overall knockdown in strength by an average of twenty three percent. This thesis proved a successful fabrication of a pristine quasi-isotropic and unidirectional panel. and unique design of an embedded defect panel at different ply surface levels for quasi-static and high strain experimental testing conditions was achieved. This design could be used for future experiments.

5.2 Potential future work

Future work can include Differential Interference contrast microscopy test for verification of the stress and to provide accurate strain measurement with the proper technique. Another idea would be to place embedded through thickness defects in unidirectional panels and test under similar conditions. More tests can be added such as a drop test or fabricating panels with different defects.

REFERENCES

1. Wu, K. Chauncey, Brian K. Stewart, and Robert A. Martin. "ISAAC-A Testbed for Advanced Composites Research." (2014).
2. Körber, Hannes. *Mechanical response of advanced composites under high strain rates*. Diss. Universidade do Porto (Portugal), 2010.
3. Li, Xin, et al. "Effect of strain rate on the mechanical properties of carbon/epoxy composites under quasi-static and dynamic loadings." *Polymer Testing* 52 (2016): 254-264.
4. Lan, Marine, et al. "Influence of embedded gap and overlap fiber placement defects on the microstructure and shear and compression properties of carbon–epoxy laminates." *Composites Part A: Applied Science and Manufacturing* 82 (2016): 198-207.
5. Fikes, John C., et al. "Composites for Exploration Upper Stage." (2016).
6. Li, Xiangqian, Stephen R. Hallett, and Michael R. Wisnom. "Modelling the effect of gaps and overlaps in automated fibre placement (AFP)-manufactured laminates." *Science and Engineering of Composite Materials* 22.2 (2015): 115-129.
7. Zhao, Han, and Gérard Gary. "On the use of SHPB techniques to determine the dynamic behavior of materials in the range of small strains." *International Journal of Solids and structures*33.23 (1996): 3363-3375.
8. Peeters, Daniël MJ, Gustavo Gonzalez Lozano, and Mostafa M. Abdalla. "Effect of steering limit constraints on the performance of variable stiffness laminates." *Computers & Structures* 196 (2018): 94-111.
9. Falcó, O., et al. "Variable-stiffness composite panels: Defect tolerance under in-plane tensile loading." *Composites Part A: Applied Science and Manufacturing* 63 (2014): 21-31.
10. Falcó, O., et al. "Effect of tow-drop gaps on the damage resistance and tolerance of Variable-Stiffness Panels." *Composite Structures* 116 (2014): 94-103.
11. Sun, Shouzheng, Zhenyu Han, and Hongya Fu. "Characteristics of stress wave propagation of carbon fiber/epoxy laminates fabricated by high-speed automated fiber placement." *Procedia CIRP* 56 (2016): 255-260.

12. Wohl, Christopher, et al. "Tack Measurements of Prepreg Tape at Variable Temperature and Humidity." (2017).

13. Van Campen, Julien MJF, Christos Kassapoglou, and Zafer Gürdal. "Generating realistic laminate fiber angle distributions for optimal variable stiffness laminates." *Composites Part B: Engineering* 43.2 (2012): 354-360.

14. Denkena, Berend, et al. "Thermographic online monitoring system for Automated Fiber Placement processes." *Composites Part B: Engineering* 97 (2016): 239-243.

15. Fayazbakhsh, Kazem, et al. "Defect layer method to capture effect of gaps and overlaps in variable stiffness laminates made by automated fiber placement." *Composite Structures*97 (2013): 245-251.

16. Pankow, M., C. Attard, and A. M. Waas. "Specimen size and shape effect in split Hopkinson pressure bar testing." *The Journal of Strain Analysis for Engineering Design* 44.8 (2009): 689-698.

17. Kim, Byung Chul, Paul M. Weaver, and Kevin Potter. "Manufacturing characteristics of the continuous tow shearing method for manufacturing of variable angle tow composites." *Composites Part A: Applied Science and Manufacturing* 61 (2014): 141-151.

18. Dirk, H-JA Lukaszewicz, Carwyn Ward, and Kevin D. Potter. "The engineering aspects of automated prepreg layup: History, present and future." *Composites Part B: Engineering* 43.3 (2012): 997-1009.

19. Denkena, Berend, Carsten Schmidt, and Patricc Weber. "Automated Fiber Placement Head for Manufacturing of Innovative Aerospace Stiffening Structures." *Procedia Manufacturing* 6 (2016): 96-104.

20. Li, Xiangqian, Stephen R. Hallett, and Michael R. Wisnom. "Modelling the effect of gaps and overlaps in automated fibre placement (AFP)-manufactured laminates." *Science and Engineering of Composite Materials* 22.2 (2015): 115-129.

21. Marouene, A., et al. "Effects of gaps and overlaps on the buckling behavior of an optimally designed variable-stiffness composite laminates–A numerical and experimental study." *Composite Structures* 140 (2016): 556-566.

22. Croft, Kaven, et al. "Experimental study of the effect of automated fiber placement induced defects on performance of composite laminates." *Composites Part A: Applied Science and Manufacturing* 42.5 (2011): 484-491.

23. Sun, Shouzheng, Zhenyu Han, and Hongya Fu. "Characteristics of stress wave propagation of carbon fiber/epoxy laminates fabricated by high-speed automated fiber placement." *Procedia CIRP* 56 (2016): 255-260.

24. Schmidt, Carsten, et al. "Influence of prepreg material quality on carbon fiber reinforced plastic laminates processed by automated fiber placement." *Procedia CIRP 67 (2018)* 67 (2018): 422-427.

25. Clancy, Gearóid J., et al. "Steering of Carbon Fiber/Thermoplastic Pre-preg Tapes using Laser-Assisted Tape Placement." *2018 AIAA/ASCE/AHS/ASC Structures, Structural Dynamics, and Materials Conference*. 2018.

26. Han, Zhenyu, et al. "Experimental Study of the Effect of Internal Defects on Stress Waves during Automated Fiber Placement." *Polymers* 10.4 (2018): 413.

27. Bakhshi, Nima, and Mehdi Hojjati. "An experimental and Simulative Study on the Defects Appeared during Tow Steering in Automated Fiber Placement." *Composites Part A: Applied Science and Manufacturing* (2018).

28. Brooks, Timothy R., and Joaquim RRA Martins. "On Manufacturing Constraints for Tow-steered Composite Design Optimization." *Composite Structures* (2018).

29. Lozano, G. Gonzalez, A. Tiwari, and C. Turner. "A design algorithm to model fibre paths for manufacturing of structurally optimised composite laminates." *Composite Structures* (2018).

30. Peeters, Daniël MJ, Gustavo Gonzalez Lozano, and Mostafa M. Abdalla. "Effect of steering limit constraints on the performance of variable stiffness laminates." *Computers & Structures* 196 (2018): 94-111.

31. Peeters, Daniël MJ, Simon Hesse, and Mostafa M. Abdalla. "Stacking sequence optimisation of variable stiffness laminates with manufacturing constraints." *Composite Structures* 125 (2015): 596-604.

VITA

ALEXANDER TROCHEZ

PROFESSIONAL EXPERIENCE

NASA LANGLEY RESEARCH CENTER, HAMPTON, VA, SEPTEMBER 2014 – PRESENT

AEROSPACE COMPOSITE ENGINEER INTERN, September 2015 to Present

- Increased understanding of working in ISO 14644-1 Clean rooms, as well as Automated Fiber Placement (AFP) equipment.
- Examined composite structures to locate delamination, cracks, breaks, holes, bulges, and determine the type and extent of repairs needed to restore original strength, repairing new parts, reinforcing, patching, replacing defective parts, applying film adhesives, and mixing two-part adhesives and sealants.
- Provide troubleshooting and correct mechanical and electrical problems on various instrumentation, equipment, and machinery.

AEROSPACE TECHNICIAN, September 2013 to August 2014

- Programmed machining by studying work orders, blueprints, engineering plans, materials, specifications, orthographic drawings, reference planes, locations of surfaces, and machining parameters; interpreted geometric dimensions and tolerances.
- Utilized familiarity with gas tungsten arc welding, gas metal arc welding, shielded metal arc welding, and Flux-core arc welding to fabricate various frames and fixtures for researchers and engineers to American Welding Society codes and procedures.
- Incorporated NASA standards and design practices including ASME Y14.1 Engineering Drawing Practices and MIL-DTL-31000B Technical Data Packages.

GRAMBLING STATE UNIVERSITY, GRAMBLING, LA, NOVEMBER 2009 TO MAY 2013

UNDERGRADUATE RESEARCH TECHNICIAN

- Carried out various duties including Polymer synthesis, wet chemistry, Anti-cancer compound synthesis, recrystallization, gravity and vacuum filtration, liquid extraction, titration, FT-IR, NMR, UV-VIS, GC-MS, Differential scanning calorimetry, Thermo Mechanical analysis, data/compound analysis, project presentations at conferences.
- Collaborated on “Properties of Aliphatic and Aromatic Polyurea-Nanoclay Composites” project.
- Served as key contributor on “Flexible Selective Estrogen Receptor Modulators” project.

UNIVERSITY OF MINNESOTA, MINNEAPOLIS, MN, SUMMER 2011

UNDERGRADUATE RESEARCH TECHNICIAN

- Analyzed oil samples on various Rheometer adapters, shear stress analysis, Trained on TA™ G-2 Rotational Rheometer, present findings to research group and principal investigator through reports and power point presentations.
- Contributed to project “Investigating End Effect Correction Factors for Rotational Viscometers.”

PUBLICATION

- Seetala, N. V., Burks, G., Hubbard, D., Trochez, A. and Khabashesku, V. N. (2012) *Positron Lifetime Analysis of Polyurea-Nanoclay Composites, in Supplemental Proceedings:* Materials Processing and Interfaces, Volume 1 (ed TMS), John Wiley & Sons, Inc., Hoboken, NJ, USA. doi: 10.1002/9781118356074.ch47